Dear Dr. Hauck,

We thank you very much for your thorough reading of our manuscript for grammatical/language issues, which we have accepted most of your suggested changes or have rephrased according to your advices. We also carefully check the entire manuscript and correct some other minor typos and mistakes. You can find all the changes in the revised final manuscript in blue and green in the track change version. The only thing we do not change as you suggested is on the use of “diel”. We intend to keep “diel” instead of replacing it with “diurnal”. According to the Merriam-Webster dictionary, “diel” involves “a 24-hour period that usually includes a day and the adjoining night”, but “diurnal” can be ambiguous since it sometimes can refer to daytime. In addition, the use of “diel” in geosciences is not uncommon (for example, Burns et al., The influence of warm-season precipitation on the diel cycle of the surface energy balance and carbon dioxide at a Colorado subalpine forest site. Biogeosciences, 12, 7349-7377, 2015).

We also thank Reviewer #1 for his/her positive comments and suggestions. We have revised the manuscript according the reviewer’s suggestions, including the improvement of the captions for Supplementary Figure 4, the addition of seasonal footprint changes which however may not influence the sign of CH_4 fluxes due to the homogeneous landscape, and the harmonization of the y-axis in Figure 4. Detailed responses to each point raised by the reviewer can be found in the attached “Responses to Reviewers” document.

We hope this revision has satisfactorily addressed all your questions and concerns and have corrected all potential problems as we can before the publication. Thank you again for your time and efforts.

Best regards,

Hanbo Yun

Responses to Reviewers

Responses to reviewer#1

1. *The new Supplementary Figure 4 clarifies wind speed and direction over the 4 seasons. I request improving the caption of Supplementary Figure 4 and explain sub-figures. I assume these stand for the 4 seasons winter, spring, summer, autumn?*

Response: Yes, you are correct that the sub-figures of Supplementary Figure 4 stand for winter, spring, summer, and autumn, respectively. In the revised manuscript, we have improved the caption by adding the sub-figure explanations.

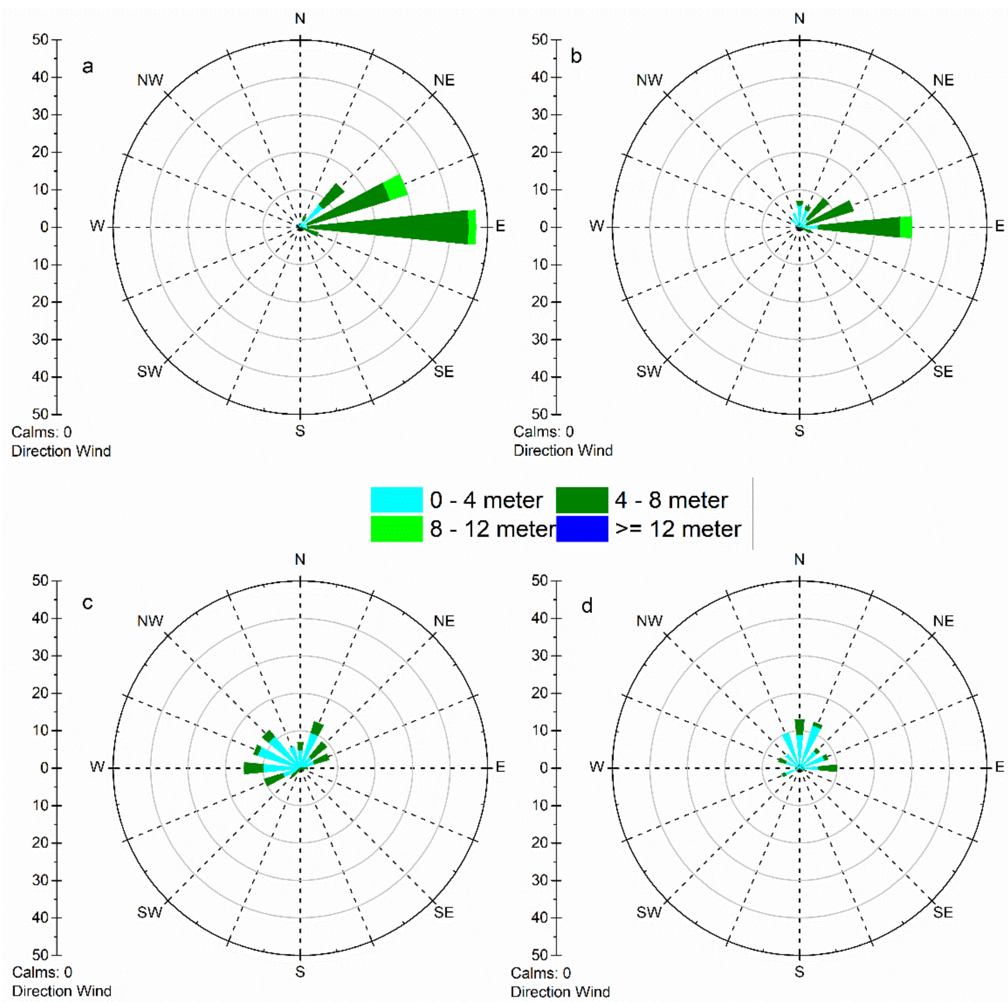

Supplementary Figure 4. Diurnal mean of wind speed and direction between 2012 and 2016: (a) is winter, (b) is spring, (c) is summer, and (d) is autumn. All data are presented as mean values with standard deviations (mean ± standard deviation).

2. If so, this figure can be used in concert with Supplementary Figure 9 in order to rule out any importance of footprint changes for the sign of the methane balance. If so, please include one sentence of text into the manuscript about it.

Response: Thank you for your constructive comments. We fully agree with the reviewer that seasonal changes in the footprint may have the potential influencing the sign of the methane balance. Following your suggestion, we have included the explicit information regarding the footprint of methane fluxes in different seasons in the revised manuscript (lines 351 – 354).

"Across different seasons the footprint of the monitored CH_4 flux changed following the change of the prevalent wind direction. In winter and spring, the major footprint was from east of the EC tower; while in summer and autumn, the major footprint was from the EC tower's west and north (Supplementary Figure 4)."

We also note in the Discussion that the footprint change may not influence the sign of methane fluxes due to landscape homogeneity in different footprints.

"Nonetheless, we found that the same vegetation species and soil exist in different directions to the tower within the footprint (Supplementary Figure 11). This spatial vegetation and soil homogeneity rules out the potential influence of footprint changes on the sign of CH_4 balances, and further confirms that seasonal soil freezing and thawing differences may likely be the main explanation for seasonal CH_4 variations." (lines 493 - 497)

3. However, the new Supplementary Figure 4 does not match the previous figure 9 about the same content - actually they show opposite wind pattern. Please, clarify!

Response: We are sorry for the confusion about the apparent difference (but they are actually the same) between the new Supplementary Figure 4 and the previous figure 9. The previous figure 9 is a wind polar figure, for which we used flow vector (wind *blowing to*) as the x-axis. In the new Supplementary Figure 4, we used the standard wind direction (wind *blowing from*). We have noted the exact meaning of wind direction in the caption of the new Supplementary Figure 4.

4. My last minor request is to harmonize the y-axis of the new Figure 4 such that the scale is equal in all sub-plots.

Response: Thanks for your constructive comments. Follow your comment, we have harmonized the y-axis of Figure 4 (copied below).

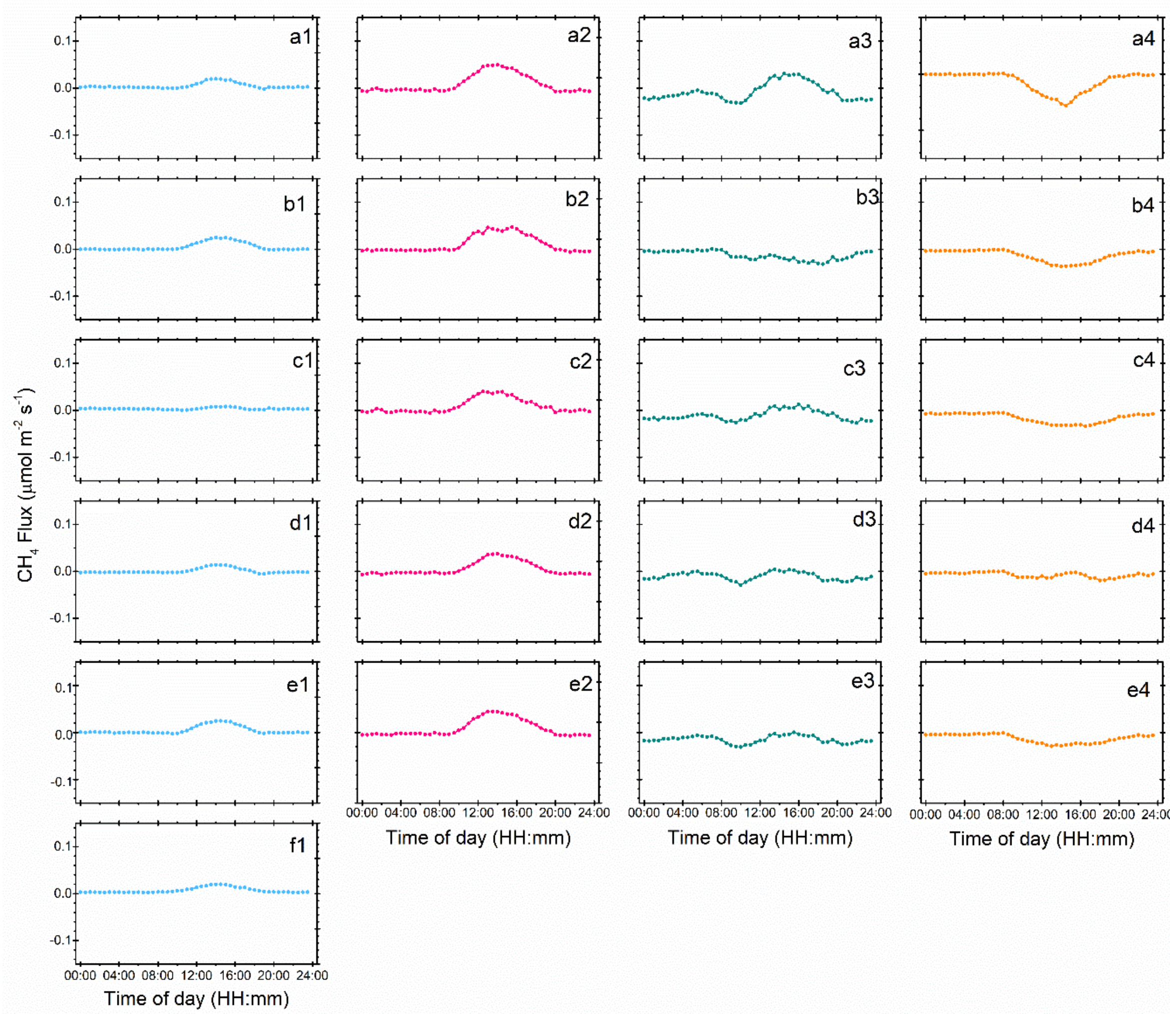

Figure 4. Diel CH_4 fluxes from 2012 to 2016 for different seasons. Blue, pink, green and orange, represent winter, spring, summer, and autumn, respectively; (a1), (a2), (a3), and (a4) are for 2012; (b1), (b2), (b3), and (b4) are for 2013; (c1), (c2), (c3) and (c4) are for 2014; (d1), (d2), (d3), and (d4) are for 2015; (e1), (e2), (e3), (e4) and (f1) are for 2016.

Consumption of atmospheric methane by the Qinghai–Tibetan Plateau alpine steppe ecosystem

Hanbo Yun[1, 2, 3], Qingbai Wu[1*], Qianlai Zhuang[3*], Anping Chen[4]* Tong Yu[3], Zhou Lyu[3], Yuzhong Yang[1], Huijun Jin[1], Guojun Liu[1], Yang Qu[3], Licheng Liu[3]

1. State Key Laboratory of Frozen Soil Engineering, Northwest Institute of Eco–Environment and Resources, Chinese Academy of Sciences, Lanzhou, Gansu 730000, China

2. Key Laboratory for Land Surface Process and Climate Change in Cold and Arid Regions, Chinese Academy of Sciences, Lanzhou, 730000, China

3. Department of Earth, Atmospheric, and Planetary Sciences, Purdue University, West Lafayette, Indiana 47907, USA

4. Department of Forestry and Natural Resources, Purdue University, West Lafayette, Indiana 47907, USA

***Authors for correspondence: qbwu@lzb.ac.cn [Q. W.]， qzhuang@purdue.edu[Q.Z], apchen1111@gmail.com [A.C.]**

A manuscript for *The Cryosphere*

May 30, 2018

Abstract

The Methane (CH_4) cycle on the Qinghai–Tibetan Plateau (QTP), the world's largest high–elevation permafrost region, is sensitive to climate change and subsequent freezing and thawing dynamics. Yet, its magnitudes, patterns, and environmental controls are still poorly understood. Here, we report results from five continuous year–round CH_4 observations from a typical alpine steppe ecosystem in the QTP permafrost region. Our results suggest that the QTP permafrost region was a CH_4 sink of -0.86 ± 0.23 g CH_4–C m^{-2} yr^{-1} over 2012 – 2016, a rate higher than that of many other permafrost areas, such as the Arctic tundra in northern Greenland, Alaska, and western Siberia. Soil temperature and soil water content were dominant factors controlling CH_4 fluxes, however, their correlations changed with soil depths, due to freezing and thawing dynamics. This region was a net CH_4 sink in autumn, but a net source in spring, despite both seasons experiencing similar top soil thawing and freezing dynamics. The opposite CH_4 source/sink function in spring versus in autumn was likely caused by the respective seasons specialized freezing and thawing processes, which modified the vertical distribution of soil layers that are highly mixed in autumn, but not in spring. Furthermore, the traditional definition of four seasons failed to capture the pattern of the annual CH_4 cycle. We developed a new seasonal division method based on soil temperature, bacterial activity, and permafrost active layer thickness, which significantly improved the modelling of the annual CH_4 cycle. Collectively, our findings highlight the critical role of fine–scale climate freezing and thawing dynamics in driving permafrost CH_4 dynamics, which needs to be better monitored and modelled in Earth system models.

1. Introduction

Since 2007, the global atmospheric methane concentration [CH_4] continues to rise, after remaining stable between the 1990s and 2006 (Rigby et al., 2008; IPCC, 2013; Patra and Kort, 2016). Understanding mechanisms for this recent increase requires improved knowledge on ~~methane (~~CH_4~~)~~ sources and sinks for regional and global CH_4 budgets (Kirschke et al., 2013; Zona et al., 2016). However, estimates on global CH_4 emissions and consumptions are still highly uncertain (Spahni et al., 2011; Kirschke, 2013). In particular, the bottom–up approach, which estimates CH_4 budgets using ground observations and inventory, overestimated the global CH_4 budget by 6～20 times, compared to the atmospherically constrained top–down approach (Zhu et al., 2004; Lau et al., 2015). This discrepancy is partly due to limited monitoring data and to our poor understanding of important factors regulating the production and consumption of CH_4 (Whalen and Reeburgh, 1990; Dengel et al., 2013; Bohn et al., 2015).

The Qinghai–Tibetan Plateau (QTP) is the world's largest high–elevation permafrost region of 1.23 ×10^6 km^{-2} (Wang et al., 2000). The QTP is currently experiencing a rapid change in climate, which affects freezing and thawing processes. The change in the freezing and thawing dynamics profoundly impacts methanotrophy and methanogenesis, which consequently impacts net CH_4 fluxes (Mastepanov *et al*., 2013; Lau et al., 2015). However, due to the scarcity of year-round ~~high temporal–resolution year–round environment and~~ ~~CH_4~~ monitoring data at high temporal resolution, we still know little about the size, seasonal pattern, and underlying controls of climate and permafrost freezing and thawing, and the resulting effects on CH_4 exchanges in the QTP permafrost region (Cao et al., 2008; Wei et al., 2015a; Song et al., 2015;). This knowledge gap also hampers our capacity to predict and understand QTP permafrost CH_4 cycles under current and projected future climates.

Here, we report results from a 5–year continuous *in situ* monitoring of CH_4 dynamics with an eddy covariance (EC) technique at the Beilu'he Research Station, which is a representative site for QTP permafrost heartland. The site was covered by alpine steppe vegetation from January 1st, 2012 to December 31st, 2016. The primary aims of this investigation are to understand (1) the long-term annual and seasonal variation of the methane budget for a typical alpine permafrost site in the QTP, and (2) the environmental factors controlling these CH_4 variations and possible underlying mechanisms. In addition, while the consumption and production of ecosystem methane are known through microbial activities, conventional investigations on seasonal methane fluxes usually used climate or vegetation defined "seasons". Therefore, a third research goal of this current study is to investigate if the classical vegetation productivity-based definition of growing season will be useful for defining the methane flux seasonality.

Formatted: Subscript

There are three advantages of our data acquisition system. First, the EC system recorded the data of CH_4 fluxes, climate, and soil properties every half hour. As the QTP permafrost is characterized by a rapidly changing climate and a rapidly changing soil freezing and thawing dynamics, even over a time period as short as one day, different aerobic or anaerobic soil environments that favor different types of CH_4 bacteria may change (Rivkina et al., 2004; Lau et al., 2015). Thus, high–resolution *in situ* monitoring data enables us to quantify CH_4 exchange patterns from ~~diel~~diurnal ~~daily~~diel to annual time–scales and investigate their major environmental drivers. Second, our field investigation spanned five full calendar years, including both plant growing and non–growing seasons. Observations of the plant non–growing season, which accounts for two-thirds of a year, ~~were~~ are very rare in current literature (Song et al., 2015). Third, the EC system we used overcame some technical problems caused by the often used static chambers, including limited representation of local site heterogeneity and additional heating of the soil surface (Chang et al., 2014; Wei et al., 2015b).

2. Methods

2.1 Site Description

The research site, Beilu'he permafrost research station (34° 09' 006" N, 92° 02' 080" E), is located in the alpine steppe continuous permafrost area of the northern QTP, about 320 kilometers southwest of Golmud, Qinghai Province (Figure 1). At an elevation of 4765 meters, the air is thin with only 0.6 standard atmospheric pressure. According to *in situ* observations, the site receives solar radiation of about ~~6720~~ 213.10 W ~~MJ~~ m~~eter~~$^{-2}$. The non–growing season is long and cold, with 225 days per year having an annual air temperature of -18 ℃ on average from 2012 to 2016. The site's growing season is short and cool, with 140 days per year from 2012 to 2016, and a mean annual air temperature of 4.6 °C. According to the site drilling exploration, the permafrost depth can extend to 50 – 70 m below ground, and the thickness of the active layer (ALT) is about 2.2 – 4.8 m (Wu et al., 2010a). The soil is composed of Quaternary fine sand or silt (Table 1), overlying on Triassic mudstone or weathered marl. Dominant plant species include: *Carex moorcroftii* Falc. *ex* Boott, *Kobresia tibetica* Maxim, *Androsace tanggulashanensis*, and *Rhodiola tibetica*. Vegetation coverage is approximately 33.5% and the average plant height is 15 cm.

Formatted: Font: Not Italic

Formatted: Font: Not Italic

Formatted: Font: Not Italic

2.2 Eddy Covariance observations

We have continuously monitored CH_4, carbon dioxide (CO_2), water (H_2O), and heat flux using a standard eddy covariance system tower 3 meters above the ground. CH_4 flux was measured with an open-path CH_4 analyzer system (Figure 1~~:~~ d; LI–7700, LI–COR Inc., Lincoln, NE, USA). The precision is 5 ppb, with RMS noise at 10 Hz and 2000 ppb. The instrument was placed on site on August 8th, 2011, and then connected to a three–dimensional sonic anemometer (heat and water flux; CSAT3, Campbell Scientific, and Logan, UT, USA; the precision is 0.1 °C~~;~~ with an accuracy ~~is~~ within 1% of reading for half–hour measurements) and an open–path infrared gas analyzer (CO_2 flux; LI–7500A, LI–COR Inc., Lincoln, NE, USA; the precision is 0.01μmol m^{-2} s^{-1} ~~and the~~with an accuracy ~~is~~ within 1% of reading for half–hour measurements, zero drift per °C is typically ± 0.1 ppm ~~typical~~) on January 1st, 2012, when the system worked steadily. Monitoring data was recorded and stored at 10 Hz using a data logger (LI–7550, LI–COR Inc., Lincoln, NE, USA).

Formatted: Not Highlight

Formatted: Not Highlight

The operation, calibrations, and maintenance of the EC system followed standard procedures. To reduce the LI–7500A surface heating/cooling influence on CO_2 and H_2O molar densities in tough environments, each year "summer style" was used in Li–7500A, in which surface temperature setting is 5 °C during May 1st to September 30th. "Winter style" was used from October 1st to the next year April 30th in Li–7500A, in which surface temperature setting is -5 °C. Calibrations of CO_2, water vapor, and dew point generator measurements for LI–7500A analyzers were performed regularly by the China Land–Atmosphere Coordinated Observation System (CLAROS). Up–and–down mirrors of LI–COR 7700 were cleaned regularly every 30 days to make sure the signal strength was stronger than 80. All of these instruments were powered by solar–panel and battery.

2.3 Micrometeorological and Soil Measurements

A wide range of meteorological variables were measured by a standard automatic meteorological tower 3 meters above the ground and 5 meters north of the eddy covariance tower. Net radiation (Rn) and albedo were measured with a four–component radiometer (Rn; CNR–1, Kipp and Zonen, the Netherlands). Air temperature (T_{air}), air relative humidity, and atmospheric pressure were measured with a temperature and humidity sensor (HMP45C, Vaisala Inc., Helsinki, Finland) in the meteorological tower. A rain gauge (TE525MM, Texas Electronics Inc., Dallas, TX, USA) was used to measure ~~the~~ precipitation~~ process~~. Wind speed and ~~wind~~ direction ~~were~~~~was~~were observed using a propeller anemometer placed on the top of the meteorological tower.

We also measured soil heat fluxes, soil temperature and soil relative water content (SWC). In August 2010, we installed ~~soil environmental~~~~these~~ sensors for soil environment and surface energy exchange monitoring 10 ~~meters~~ m apart from the eddy covariance tower~~, for EC surface energy balance ratio evaluating.~~~~soil sample collection.~~ Two self–calibrating soil heat flux (SHF) sensors (HFP01) were placed 5 cm and 15 cm below the ground. A group pF–Meter sensor (GEO–Precision, Germany) was embedded in the soil under the meteorological tower to measure soil temperature (T_{soil}) at 0 cm, 5 cm, 10 cm, 15 cm, 20 cm, 30 cm, 40 cm, 50 cm, 70 cm, 80 cm, 100 cm, 150 cm, 160 cm, and 200 cm depth. The pF meter sensors also measured SWC at 10 cm, 20 cm, 40 cm, 80 cm, and 160cm depth.

Formatted: Highlight

Formatted: Highlight

Formatted: Highlight

Formatted: Highlight

All of above environmental parameters were synchronously monitored with eddy covariance, and the data was recorded every 30 minutes by CR3000 (Data logger, Campbell Data Taker Ltd, Salt Lake City, UT, USA). The air temperature sensors, the humidity sensors, and the pF meter sensors were calibrated in the State Key Laboratory of Frozen Soil Engineering at the Chinese Academy of Sciences in order to ensure the measurement accuracy was within ± 0.05 °C and ± 5%, respectively.

We also sampled soil profiles for soil physical and chemical measurements with one 1 m~~eter~~ × 1 m~~eter~~ × 2~~-~~ m~~eter~~ pit 10 m~~eter~~ apart from the eddy covariance tower in August 2010.

Five profile samples were taken from the pit at depths 0 − 20 cm, 20 − 50 cm, 50 − 120 cm, 120 − 160 cm, and 160 − 200 cm. Sampling at each depth was repeated five times and the samples of the same depths were then well mixed. ~~Every depth was repeated five times after being fully mixed.~~ ~~Then~~ After that, the mixed soil sample of each depth ~~each depth~~ was stored in ~~soil sample~~ aluminum boxes and carefully sealed to prevent gas exchanges with air. The clod method was used to investigate the field wet bulk density (weight of soil per unit volume; Cate and ~~nelson~~Nelson, 1971). The soil moisture content was calculated gravimetrically by the ratio of the mass of water present to the oven–dry (60 °C for 24 hour) weight of the soil sample. The soil organic carbon (SOC) content of the air–dried soil samples was analyzed using the wet combustion method, Walkley–Black modified acid dichromate digestion, $FeSO_4$ titration, and an automatic titrator. Total nitrogen (TN) and pH were measured using standard soil test procedures from the Chinese Ecosystem Research Network.

To understand the potential effect of soil thawing and freezing dynamics on CH_4 fluxes, we also reconstructed and verified semi-monthly data of soil active layer thickness (ALT). Following Muller's original definition, ALT is the maximum thaw depth in the late autumn using a linear interpolation of T_{soil} ~~(temperature of soil)~~ profiles between two neighboring points above and below the 0 °C isotherm (Muller, 1947). We used records of the soil thawing thickness measured with a self–made geological probe to verify the ALT data semi–monthly. More information about the measurement procedure was previously described by Wu and Zhang (2010a).

2.4 Microbial Activity

To understand how soil microbial activity may have impacted the CH_4 fluxes, we sampled 100 ~~-~~g~~ram~~ soils for soil microbial activity measurements. These soils were obtained using a soil

Formatted: Highlight

Formatted: Subscript

sample drill device (Ø=0.03 m), with depths of 0 − 25 cm taken every 5 days within 100 m of the eddy covariance tower. The sampled soil was fully mixed and divided into two equal parts. Each part was then stored in sterilized aluminum boxes and then placed in liquid nitrogen, before sending to the lab for microbe RNA extraction. We then used a real-time PCR method to genetically test methanotrophic / archaeal methanogens, and the procedure was repeated three times for each sample. By setting the maximum methanotrophic / archaeal methanogens gene expression cyclic number as 1, we calculated the variety coefficient of methanotrophic and archaeal methanogens gene expressions (ΔI and ΔII, respectively; %) with equation (1):

$$\Delta_i = {}^{X_I}\!/\!{}_{X_{Max}} \quad \ldots \quad (1)$$

Δ_i is for the i[th] methanotrophic/archaeal methanogens gene expression; X_i is the methanotrophic / archaeal methanogen gene expression cyclic number of the i[th] time; X_{Max} is the maximum methanotrophic / archaeal methanogen gene expression cyclic number of the soil group from 2012 to 2016.

2.5 EC Data Processing and Data Filtering

Data collected from January 1[st], 2012 to December 31[st], 2016 was used in this study. Before processing, we removed data that was recorded at the time of precipitation events or with LI–7700 signal strength under 85. We first processed the raw data in ~~Eddypro~~ EddyPro (version 6.2.0, ~~(~~LI–COR, Lincoln, NE, USA). We adopted standardized procedures recommended in Lee et al. (2006) to process half–hourly flux raw measurements to ensure their quality.

1) Data was processed through statistical analysis in ~~Eddypro~~ EddyPro ~~6.2.0~~ including:

spike removal (accepted spikes < 5% and replaced spikes with linear interpolation), amplitude resolution (range of variation: 7.0 σ, number of bins: 100, accepted empty bins: 70%), drop–outs (percentile defining extreme bins: 10, accepted central drop–outs: 10%, accepted extreme drop–outs: 6%), absolute limits (-30 m s^{-1} < U < 30 m s^{-1}, -5 m s^{-1} < W < 5 m s^{-1}, -40 °C < Ts < 40 °C, 200 μmol mol^{-1} < CO_2 < 500 μmol mol^{-1}, 0 μmol mol^{-1} < H_2O < 40 μmol mol^{-1}, 0.17 μmol < CH_4 < 1000 μmol), Skewness and kurtosis (-2.0 < Skewness lower limit < -1.0, 1.0 < Skewness up limit < 2.0; 1.0 < Kurtosis lower limit < 2.0, 5.0 < Kurtosis upper limit < 8.0), discontinuities (hard–flag threshold: U = 4.0, W = 2.0, T_S = 4.0, CO_2 = 40, CH_4 = 40, and H_2O = 3.26; soft–flag threshold: U = 2.7, W = 1.3, T_S = 2.7, CO_2 = 27, CH_4 = 30, and H_2O = 2.2), angle of attack (minimum angle of attack = -30, maximum angle attack = 30, accepted amount of outliers = 10%), and steadiness of horizontal wind (accepted wind relative instationarity = 0.5) (Vickers and Mahrt, 1997; Mauder et al., 2013).

Formatted: Font color: Auto

2) The data was then corrected using atmosphere physical calculations expressed by: axis rotations of tilt correction (double rotation), time lags compensation (covariance maximization), and compensating density fluctuations of Webb–Pearman–Leuning ~~(WPL)~~ (Webb et al., 1980)~~terms~~. When CO_2 and H_2O molar densities are measured with the LI–COR 7500 / LI–COR 7500A in cold environments (low temperatures below -10 °C), a correction should be applied to account for the additional instrument–related sensible heat flux, due to instrument surface heating / cooling. Thus, we implemented the correction according to Burba et al. (2008), which involves calculating a corrected sensible heat flux (*H'*) by adding estimated sensible heat fluxes from key instrument surface elements, including the bottom window (H_{bot}), top window (H_{top}), and spar (H_{spar}) to the ambient sensible heat flux (*H*):

Formatted: Font: (Default) Times New Roman, 12 pt, Font color: Text 1, (Asian) Chinese (PRC)

$$H'=H+H_{bot}+H_{top}+0.15\times H_{spar} \quad (2)$$

3) Quality assurance (QA) / quality control (QC) were ensured through spectral analysis and corrections analysis in ~~Eddypro~~ EddyPro~~6.2.0~~. Spectra and co–spectra calculations used power–of–two samples to speed up the Fast Fourier Transform (FFT) algorithm. Here we checked the “Filter (co)spectra according to Vickers and Mahrt (1997) test results” box in EddyPro, which would then disregard EC flux time series that would likely create artifacts in spectral and co-spectral shapes~~Spectra and co–spectra QA / QC by filter were made according to Vickers and Mahrt (1997) to test EC dataresults,~~ . ~~and~~ We ~~then~~also used the Mauder and Foken (2004) micrometeorological quality tests embedded in EddyPro to filter low quality~~for~~ EC time series data~~data deeply test results~~. Low–frequency range spectral correction was done considering high–pass filtering effects. High–frequency range spectral correction was done considering low–pass filtering effects (Moncrieff et al., 2004).

Formatted: Highlight

4) We chose values of “0”,”1”, “2” to flag the processed flux data into three quality classes in Eddy~~p~~Pro~~ 6.2.0~~. The combined flag attains the value “0” for best quality fluxes, “1” for fluxes suitable for general analysis, such as annual budgets, and “2” for fluxes that should be discarded from the results dataset. For our dataset, approximately 67% of the data fell into Class 0, 12% in Class 1, and 21% in Class 2.

5) Our analysis indicated that, under average meteorological conditions, 80% of the flux (footprint) came from an area within 175 m of the eddy covariance tower.

In addition, we also adopted the method in Burba et al. (2008) to adjust the half–hour flux data, to avoid apparent ~~measuring~~ measurement errors. In doing this, we rejected half–hour flux data that fell into one of the following situations: (1) incomplete half–hour measurements, (2) measurements under rain impacts, (3) nighttime measurements under stable atmospheric conditions (~~U*,~~ friction velocity~~,~~, U* < 0.1 m s^{-1}), and (4) abnormal values detected by a three–dimensional ultrasonic anemometer. This screening resulted in the rejection of about 20.7% of all the ~~all~~ flux data.

After the above data quality control, there was a 28.7% data gap for CH_4 fluxes over the entire ~~examination~~ period. These data gaps were then filled according to the method described in literature (Falge et al., 2001; Papale et al., 2003). We used a linear interpolation to fill the gaps if they were less than 2 hours, a method described in Falge *et al*. (2001) to fill gaps greater than 2 hours, but less than 1 day, and an artificial neural network approach as described in Papale et al. (2003) and Dengel et al. (2013) to fill gaps greater than 1 day.

The quality of the dataset was evaluated using the equation of energy closure:

$$EBR = \sum (H + \lambda E) / \sum (R_n - G - S) \quad (3)$$

where the *EBR* is surface energy balance ratio~~;~~, *H* is heat flux~~; λE~~, λE is latent heat~~;~~, *Rn* is net radiation~~;~~, *G* is soil heat flux (SHF~~);~~), and *S* is heat storage of the vegetation canopy. As vegetation coverage at this research site is sparse, *S* is ignored. From 2012 to 2016, the~~ ~~ average *EBR* ~~average~~ value at the Beilu'he EC site was ~~larger than~~about ~~67.5%~~0.675~~ in this study~~, falling within the range of 0.34 to 1.69 in an analysis of energy balance closure for global FLUXNET sites (Wilson et al., 2002).

We analyzed two different major sources of CH_4 flux gap–filling uncertainty. The first kind of uncertainty came from U* threshold estimate. Following Burba et al. (2008), we excluded the probably false low CH_4 flux at low U*. However, it was difficult to determine the value for the U* threshold. For instance, when choosing a lower U* threshold, the associated

Field Code Changed

Formatted: Highlight

Formatted: Highlight

Formatted: Highlight

Formatted: Highlight

Formatted: Highlight

lower flux would contribute to the gap filling and the annual gross (Loescher, et al., 2006). Here we used ~~T~~the variance from 5% to 95% of the bootstrapped values to provide~~d~~ ~~an average of~~an estimate on the uncertainties caused by ~~the~~ different U^* ~~to filter out~~thresholds. The second uncertainty source was due to insufficient power supply. In this research, all instrument power was supplied by solar panels. Extended periods of rainy, cloudy, and snowy weather ~~,~~ would cause the instrument to stop working due to an insufficient power supply. When we used the ~~method to fill the gap~~gap-filling method mentioned above, it would cause the CH_4 flux to deviate from the true value. To our knowledge, the CH_4 flux data was largely uncertain under rainy conditions.

Formatted: Highlight

2.6 ~~Based on microbial activities classification~~ New classification system of the four seasons based on microbial activities classification

We redefined the four seasons of ~~spring~~ spring, ~~summer~~ summer, ~~autumn~~ autumn, and ~~winter~~ winter~~, and~~ based on the microbial activity parameters of the new seasons ~~on microbial activities~~ (Figure 2), ALT ~~variety~~ variability coefficients (ALT variability~~variety~~ coefficient = $(ALT_{i+1} - ALT_i) / ALT_{Max}$, where ALT_{Max} is the maximum of ALT per year), and T_{soil}. Below, we describe the start date of each season (~~The~~ the end date of a season is the day immediately before the start of the next season).

Formatted: Subscript

~~Spring~~ Spring starts at the first day of two consecutive observation periods fulfilling both (1) $(\Delta II + \Delta I) / 2 \geqslant 15\%$, and (2) the ALT variability~~variety~~ coefficient $\geqslant 0.05$.

~~Summer~~ Summer starts on the first day of two consecutive observation periods when (1) $(\Delta II + \Delta I) / 2 \geqslant 45\%$, (2) ALT variability~~variety~~ coefficient $\geqslant 0.35$, and (3) five successive days with T_{soil} at 40 cm soil depth $\geqslant 0$ °C.

Formatted: Subscript

~~Autumn~~ Autumn starts on the first day of two consecutive observation periods when (1) $(\Delta II + \Delta I) / 2 \geqslant 55\%$, (2) the ALT variability~~variety~~ coefficient $\geqslant 0.60$, and (3) five successive days the T_{soil} of 10 cm < 5 °C.

~~Winter~~ Winter starts on the first day of two consecutive observation periods that (1) $(\Delta II + \Delta I) / 2 < 15\%$ and the ALT variability~~variety~~ coefficient < 0.05.

To test the robustness of our new seasonal division method in our methane cycle analysis, we compared empirical CH_4 flux estimates using different season definitions (Table 2). In addition to our new method that was based on top soil microbe activity, T_{soil} of 0 – 40 cm, and permafrost active layer variability (hereafter refer to as SMT), we also used three conventional methods, ~~one~~ based on (i) vegetation cover and temperature change (VCT), (ii) based~~one~~ on Julian months (JMC), and (iii) based~~the other one~~ on vegetation phenology change (VPC). ~~Specifically, the~~ The VCT method splits a year into a plant growing season and a non–growing season; the JMC method assumes May to October as a plant growing season, and November to the following April as a non–growing season; and the VPC method defines a plant growing season as the period between the time when all dominant grass species (*Carex* ~~*Moorcroft*~~ *moorcroftii* Falc. *ex* Boott, *Kobresia tibetica* Maxim, *Androsace tanggulashanensis*, *Rhodiola tibetica*) germinate and that when they all senesce.

2.7 Statistical Analyses

To understand the connections between CH_4 fluxes and associated environmental factors, we performed a series of statistical analyses, including correlation, principal component analyses (PCA), and linear regression analyses, in IBM SPSS (IBM SPSS Statistics 24; IBM, Armonk NY, USA). Specifically, we used bivariate correlation to examine pairwise relationships between

Formatted: Subscript

Formatted: Subscript

Formatted: Font: Not Italic

Formatted: Font: Not Italic

Formatted: Font: Not Italic

environmental factors and CH_4 fluxes. We also used PCA and linear regressions to explore the sensitivity of CH_4 fluxes to simultaneous environmental fluctuations in wind speed, T_{air}, air relative humidity, Rn, vapor pressure deficit (VPD), albedo, SHF, SWC, and T_{soil}. Before performing PCA and linear regressions, the entire dataset was examined for outliers (Cook's Distance, < 0.002), homogeneity of variance (Levene test, $p < 0.05$), normality (Kolmogorov–Smirnov test, smooth line for histogram of Studentized residuals), collinearity (variance inflation factor, 0 < VIF < 10), potential interactions (*t*–test, $p < 0.05$), and independence of observations (*t*–test, $p < 0.05$).

Formatted: Subscript

Formatted: Subscript

We performed structural equation modeling (SEM) to evaluate the effects of environmental variables on CH_4 fluxes for different seasons. SEM is a widely-used multivariate statistical tool that incorporates factor analysis, path analysis, and maximum likelihood analysis. This method uses *priori* knowledge of the relationships between focus variables to verify the validity of hypotheses. Here we performed SEM analyses with AMOS 21.0 (Amos Development Corporation, Chicago, IL, USA). All data are presented as mean values with standard deviations.

3. Results

3.1 Meteorological Conditions

We first reported the statistics of the meteorological conditions environmental factors at the Beilu'he Permafrost Weather Station based on meteorological records frombetween 2012 to 2016. Mean annual T_{air} was -4.5 ℃ (Supplementary Figure 1), with minimum and maximum mean dieldiurnaldiel temperatures of -21.6 ℃ (12th January, 2012) and 13.8 ℃ (28th July, 2015), respectively. Average net radiation was 82.8 Wm^{-2}, while with the maximum was in August (136.2 Wm^{-2}; Supplementary Figure 2). The average VPD was about 0.3, while thewith

Formatted: Subscript

maximum and minimum values of ~~was~~ 0.98, and ~~the minimum was~~ 0.02, respectively (Supplementary Figure 3). Mean annual precipitation was 335.4 mm (Figure 3), which was primarily based on rain and snowfall (only occupied 7%). Maximum and minimum~~From 2012 to 2016, the maximum~~ precipitation was encountered in 2013 (488.3 mm), and ~~the minimum was in~~ 2015 (310.0 mm), respectively. The majority of precipitation, approximately 92%, occurred hereby in the summer. During the winter, precipitation was rare ~~and the~~with mean values ~~was about~~around 6.7 mm~~, with the value decreasing even further from 14.2 mm in 2012, to 2.1 mm in 2016~~. Spring was another important rainfall period besides summer, with mean precipitation being about 37.5 mm, or 8～17% of the total.

The Beilu'he site is windy during most of the year (Supplementary Figure 4). Its annual average speed was 4.4 m s^{-1} from 2012 to 2016~~, while its maximum and minimum wind speeds were 14.6 m s^{-1} on 14th February, 2016 and 1.3 m s^{-1} on 1st November, 2013, respectively. Its winter, spring, and autumn average wind speed were 5.4 m s^{-1}, 4.3 m s^{-1}, and 3.7 m s^{-1}, respectively~~, while the principal direction of the strongest winds were from the southwest. Late autumn, winter, and early spring drought brought increased risks of dust blowing days, with an average of 122 days within a year. Its summer average wind speed was about 3.30 m s^{-1}, predominantly driven by the southwest wind.

The SWC and T_{soil} ~~varieties~~ variability ~~of soil layers~~ from 2012 to 2016 at the field site ~~were~~ are summarized in Supplementary Figures 5 and ~~Supplementary Figure~~ 6, respectively. Mean SWC of depths 10 cm, 20 cm, 40 cm, 80 cm, and 160 cm were 14%, 9%, 8%, 14%, and 19%, respectively. T_{soil} of depths <100 cm ~~0 cm, 5 cm, 10 cm, 20 cm, 30 cm, 40 cm, 50 cm, 70 cm, and 80 cm~~ corresponded with the T_{air} changes, but showed stronger differences at

Formatted: Subscript

Formatted: Subscript

Formatted: Subscript

depths ≥100 cm~~., 150 cm, 160 cm, and 200 cm did not correspond.~~ The T_{soil} ~~of depth~~at 200 cm depth showed ~~had~~ a remarkable difference from ~~the T_{soil}~~that of other layers. The reason could be the occurrence of~~that~~ peat ~~existed~~ in this layer, and that, during winter, the peat layer was not completely frozen. Supplementary Figure 7 shows SHF half-hour and ~~diel~~~~diurnal~~ diel scale ~~varieties~~variability of 5 cm and 15 cm depth. The annual mean value of SHF at 5 cm and 15 cm depth is 7.6 W m^{-2} and 6.8 W m^{-2}, respectively.

Finally, ~~we also reported~~ Supplementary Figure 8 shows the site's average soil freezing and thawing dynamics observed from January 2012 to December 2016. ~~in Supplementary Figure 8. The duration of the active layer in the thawing state at~~ The average ALT is 4.4 m from 2012 to 2016. At 40 cm depth the duration of the active layer ranged from 174 to 188 days, with an average variation of up to 14 days. ~~The average ALT is 4.4 m from 2012 to 2016.~~

3.2 Annual, Seasonal and ~~Diel~~~~Diurnal~~ Diel Variabilities of Methane Fluxes

Our results indicated that the Beilu'he site was a CH_4 sink, with an annual mean strength of -0.86 ± 0.23 g CH_4–C m^{-2} (95% confidence interval; negative values mean CH_4 sinks, positive values mean CH_4 sources). The strength of the CH_4 sink varies across different years from -0.57 ± 0.27g CH_4–C m^{-2} yr^{-1} in 2015, to -1.49 ± 0.38g CH_4–C m^{-2} yr^{-1} in 2014 (Figure 3). The amount of gene expression by methanogens and methanotrophs at 0 − 25 cm soils in March and November, for instance, were about 16.8% and 35.6%, respectively, suggesting strong microbial activities even during the cold and dry plant non–growing season (Figure 2).

We also clearly observed CH_4 seasonal variations (Supplementary Figure 9) in both the amount of CH_4 exchanges and their ~~diel~~~~diurnal~~diel cycles (Figure 4). ~~The~~Across different seasons the footprint of the monitored ~~methane~~CH_4 flux ~~footprint area is~~ changes~~d~~ ~~from a~~

Formatted: Subscript

Formatted: Subscript

Formatted: Subscript

differentfollowing the change of the prevalent wind direction. In winter and spring, the major footprint iwas from east of the EC tower,; while in summer and autumn, the major footprint iswas from the EC tower's west toand north (sSupplementary fFigure 4).

In winter winter, the net CH_4 flux at the Beilu'he site was an atmospheric source, with an average annual rate of 0.41 ± 0.16 g CH_4–C m^{-2} yr^{-1} or 4.35 ± 0.33 mg CH_4–C m^{-2} d^{-1} (Supplementary Figure 9: a). It should also be noted that since the investigation started January 1st, 2012, and ended on December 31st, 2016, the 2011 ～ 2012 and 2016 ～ 2017 winters were only about half of the regular length. The dieldiurnaldiel CH_4 cycle of an average winter winter day was characterized by one single emission peak around 10:30am ～ 17:30 pm (Figure 4: a1-4f1, b1, c1, d1, e1 and f1).

In spring spring, the Beilu'he site was a CH_4 source of 0.90 ± 0.37 g CH_4–C m^{-2} yr^{-1} (Supplementary Figure 9: b), accounting for 53% of annual CH_4 emissions, or 1.81 ± 0.22 mg CH_4–C m^{-2} d^{-1}. For a typical spring spring day (Figure 4: a2, b2, c2, d2, and 4 e2), dieldiurnaldiel CH_4 emission usually started at around 10:00 am ～ 10:30 am, when the thin ice layer on the soil surface started to thaw. It then reached the peak at 12:30 pm ～ 13:30 pm. The emission peak started to weaken at around 15:30 pm ～ 16:00 pm and reached around zero or even turned into a small sink after 20:00 pm.

In summer summer, the Beilu'he site was a CH_4 sink of -0.99 ± 0.18 g CH_4–C m^{-2} yr^{-1} (Supplementary Figure 9: c), or -13.28 ± 0.38 mg CH_4–C m^{-2} d^{-1}. The dieldiurnaldiel cycle of CH_4 fluxes in summer summer was characterized with two absorption peaks and one small emission peak (Figure 4: a3, b3, c3, d3, and 4e3). With T_{air} increasing after sunrise, the soils started to absorb atmospheric CH_4 and this soil uptake process reached its first peak at around

Formatted: Subscript

9:30 am ~ 10:30 am. After that, the continuously increasing T_{air} turned to suppress CH_4 uptake and promote CH_4 emissions, likely due to different temperature sensitivities of methanotrophic and methanogenic bacteria. At around 15:30pm ~ 16:00 pm, when T_{air} reached the maximum (Supplementary Figure 1: b), CH_4 emission also reached its peak. The following temperature decrease in the late afternoon again reversed the CH_4 uptake / emission process, and by sunset we observed another CH_4 sink peak. The rate of CH_4 sink then decreased again through the night with further decreasing temperature.

Autumn Autumn was another season with a net CH_4 sink, with the season having the highest observed value for the site as a CH_4 sink in 2013 (Supplementary Figure 9: d). The CH_4 sink in autumn autumn varied between -0.69 ± 0.19 g CH_4–C m^{-2} (2015), and -1.59 ± 0.33 g CH_4–C m^{-2} (2013), with an average dieldiurnaldiel rate of -1.19 ± 0.48 g CH_4–C m^{-2} yr^{-1} or -13.31 ± 0.28 mg CH_4–C m^{-2} d^{-1}. The dieldiurnaldiel dynamics of autumn autumn CH_4 fluxes was like a letter "V", with a single sink peak during 13:30 pm ~ 15:30 pm (Figure 4: a4, b4, c4, d4, and 4e4).

3.3 Response of Methane Fluxes to Changes in Environmental Factors

DielDiurnalDiel fluxes of CH_4 were highly correlated with many biotic and abiotic environmental factors, either positively or negatively (Table 3). Positive factors include metagenomics of both methanotrophic (r = 0.52, $p < 0.01$) and methanogens (r = 0.49, $p < 0.01$) at 0 − 25 cm soils, ALT (r = 0.43, $p < 0.01$), and wind speed (r = 0.15, $p < 0.01$). Important negative factors include VPD (r = -0.26, $p < 0.01$), SWC at all depths (varied r values between -0.17 and -0.26, $p < 0.01$), T_{air} (r = -0.11, $p < 0.01$), and air pressure (r = -0.15, $p < 0.01$). The correlation signal between CH_4 fluxes and T_{soil} changed with soil depths (varied r values between -0.09 and 0.24, $p < 0.01$). Furthermore, path analysis results showed that T_{soil} at 5cm and 10cm

Formatted: Subscript

Formatted: Subscript

Formatted: Subscript

Formatted: Subscript

Formatted: Subscript

were the most important factors, which together contributed about 25% of the relative importance coefficient. Following these factors in importance were SWC at 80 cm (14%) and 20 cm (12%), and T_{soil} at 20 cm (8%).

Further analyses suggested that dominant control factors of CH_4 fluxes also changed among different seasons. In ~~spring~~ spring, Rn was the most important factor, with a relative importance coefficient near 60%, followed by SHF at 5 cm (9%), and SWC at 20 cm (6%). Table 4 shows the results of the PCA. In ~~spring~~ spring, PC1 explained 63% of the CH_4 variations, which was positively correlated with T_{air}, VPD, Rn, SHF of 15 cm, ALT, ΔI, SWC of 10 – 40 cm, T_{soil} of 0 cm, T_{soil} of 5 – 20 cm, T_{soil} of 30 – 50 cm, and negatively correlated with wind speed. The PC2 explained about 23% of CH_4 fluxes variations. ~~PC2 was positively correlated with wind speed, Tair, Rn, SHF of 15cm, but negatively correlated with VPD, ALT, ΔI, SWC 10 – 40 cm, Tsoil of 0 cm, Tsoil of 5 – 20 cm, and Tsoil of 30 – 50 cm.~~ The first four principal components explained about 86% of the CH_4 variations.

In ~~summer~~ summer, CH_4 fluxes were mostly related with T_{soil} at 100 cm and 200 cm, with an relative importance coefficient of about 30.2% and 26.5%, respectively. Other important environmental determinants of CH_4 fluxes were T_{soil} at 70 cm (12.3%), and T_{soil} at 0 − 20 cm (11.4%). The first four principal components explained about 88% of the CH_4 variations (Table 4). PC1 explained 70% of the CH_4 variations~~. PC1~~ and was positively correlated with wind speed, T_{air}, VPD, SHF of 15 cm, ALT, ΔI, SWC of 50 – 160 cm, precipitation, T_{soil} of 0 cm, T_{soil} of 5 – 40 cm, T_{soil} of 50 – 80 cm, and T_{soil} of 100 − 200 cm, but negatively correlated with Rn and SWC of 10 − 40 cm. ~~PC2 was positively correlated with wind speed, Tair, VPD, Rn, SHF of 15cm, SWC of 10 – 40 cm, Tsoil of 0 cm, but negatively correlated with ALT, ΔI, SWC of 50 – 160 cm, precipitation, Tsoil of 5 – 40 cm, Tsoil of 50 – 80 cm, and Tsoil of 100 – 200 cm.~~

In ~~autumn~~ autumn, Rn and T_{soil} at 5 − 20 cm had the highest relative importance coefficients for explaining the CH_4 flux variation. The first four principal components explained about 86% of the CH_4 variations (Table 4). PC1 explained 69% of the CH_4 variations~~. PC1~~ and was positively correlated with T_{air}, VPD, Rn, SHF of 15 cm, ALT, ΔI, SWC of 10 – 40 cm, SWC of 50 – 160 cm, T_{soil} of 0 cm, T_{soil} of 5 – 40 cm, T_{soil} of 50 – 80 cm, and T_{soil} of 100 – 200 cm, but negatively correlated with wind speed. ~~PC2 was positively correlated with wind speed, Tair, Rn, SHF of 15 cm, ALT, ΔI, Tsoil of 0 cm, and Tsoil of 5 − 40 cm, but negatively correlated with VPD, SWC of 10 − 40 cm, SWC of 50 − 60 cm, Tsoil of 50 − 80 cm, and Tsoil of 100 − 200 cm.~~

During ~~winter~~ winter, Rn was again the most important factor (34% relative importance coefficient), followed by T_{soil} at 0 − 40 cm (27% in total), and SHF of 15 cm (17% in total), in determining CH_4 fluxes. The first four principal components explained about 96% of the CH_4 variations (Table 4). PC1 explained 75% of the CH_4 variations~~. PC1~~ and was positively correlated with wind speed, T_{air}, VPD, Rn, SHF of 15 cm, ΔI, T_{soil} of 0 cm, and T_{soil} of 5 − 20 cm. ~~PC2 explained 21% of the CH_4 variations. PC2 was positively correlated with wind speed, Tair, Rn, SHF of 15 cm, and ΔI, but negatively correlated with VPD, Tsoil of 0 cm, and Tsoil of 5 − 20 cm.~~

3.4 Empirical Model Comparison for Different CH_4 Flux Season Classification System

Lastly, we also compared how different season definitions, including the methods of SMT, VCT, JMC, and VPC, may have impacted the predictbility of CH_4 fluxes. We established empirical maximum likelihood models between all environmental factors and ~~diel~~~~diurnal~~diel CH_4 fluxes over each season, and then compared modeled CH_4 fluxes and field observations under those methods of different seasonal definitions (Figure 5). We found that the agreement between modeled and observed CH_4 fluxes, using the new SMT method, reached $R^2 = 0.28$, almost twice -that of the VPC ($R^2 = 0.17$) and VCT ($R^2 = 0.14$) methods, and more than three times that of the JMC method ($R^2 = 0.08$; Figure 5). Hence, the comparison suggested that our new method could better model CH_4 fluxes over a year. The use of the traditional plant growing season versus nongrowing season definitions may also underestimate or overestimate CH_4 sinks or sources, especially when many studies assume CH_4 is close to zero during the plant nongrowing season. Furthermore, the new SMT method accurately captures the impact of spring–springm and autumn–autumnm permafrost thawing / freezing cycles on CH_4 fluxes, and the different preferable environments for methanogens and methanotrophic bacteria during the summer–summerm season, while conventional methods do not.

4. Discussion

4.1 Annual, Season mean and DielDiurnalDiel Variability

Our results suggested that the alpine steppe ecosystem in Beilu'he was a CH4 sink of about -0.86 ± 0.23 g $CH_4 - C\ m^{-2}\ yr^{-1}$ during the study period of 2012-2016. This sink strength is larger than that of previous reports from other sites of the QTP (Cao et al., 2008; Wei et al., 2012; Li et al., 2012; Song et al., 2015; Chang and Shi, 2015), and many other high-latitude Arctic tundra ecosystems, like northeast Greenland (Jørgensen et al., 2015), western Siberia (Liebner et al., 2011), and Alaska (Whalen et al., 1992; Zhuang et al., 2004; Whalen, 2005). Different soil hydrothermal conditions, which previous studies have shown will greatly influence CH_4 cycles in permafrost regions (Spahni et al., 2011; Kirschke et al., 2013), may partly explain the site difference in CH_4 dynamics. For example, compared to the wet and often snow–covered high–latitude Arctic tundra ecosystems, there is no or little snow cover during the cold season in the QTP alpine steppes (Supplementary Table 1). During winter–winter, the Beilu'he meteorological data shows that the snow-cover time < 33.7h, SWC of 0-40cm within footprint < 7.6% from 2012 to 2016 (Supplementary Table 1) , is far below high–latitude Arctic tundra ecosystems. Jansson and Taş (2014) pointed out that relatively dry soils could faciliate the oxidation of CH_4, since the increased number of gaps between soil particles in dry soils enhances the diffusion of oxygen (O_2) and CH_4 molecules and promotes aerobic respiration of soil microorganisms (Wang et al., 2014; Song et al., 2015). Meanwhile, unfrozen or capillary water found in cold–season permafrost soils ensures sufficient soil moisture for microbial activities, even in relatively drier and cold soils (Panikov and Dedysh, 2000; Rivkina et al., 2004). In addition, many previous studies used static chambers in CH_4 measurements, and may not have included a plant non–growing season (Wei et al., 2015a; Wang et al., 2014). Static chambers could underestimate CH_4 uptake because of the additional chamber heating-induced CH_4 emissions and frequent measurement gaps from overheating preventive shutdowns (Sturtevant et al., 2012).

We argued that seasonal freezing and thawing dynamics may be a key reason to explain the site's seasonal difference in CH_4 dynamics. Freezing and thawing processes are typical characteristics of the QTP permafrost (Wang et al., 2008; Wang et al., 2000; Qin et al., 2016). Our work suggests that freezing and thawing dynamics have played a critical role in governing permafrost seasonal and dieldiurnal diel CH_4 cycling. For instance, while both spring spring and autumn autumn are active seasons for the freeze-thaw dynamics of top soil layers and share many similarities, they have opposite CH_4 processes–soils emit CH_4 during spring spring (Supplementary Figure 9: b), but consume CH_4 during autumn autumn (Supplementary Figure 9: d). We hypothesize that the difference in the freezing and thawing processes of the two seasons may have played a critical role in determining the direction of CH_4 dynamics. In

~~spring~~ spring, the SWC of 10 cm, ~~is 12.4%,~~ of 20-40 cm ~~is 9.2%,~~ of 80 cm ~~is 11.4%,~~ and of 160 cm depth is 12.4%, 9.2%, 11.4%, and 13.6%, respectively (Supplementary Table 1~~),~~). ~~the~~ The active soil layer thaws from top to bottom (Jin et al., 2000; Cao et al., 2017), and the permafrost table is very shallow (about 10 ～ 45 cm)~~, and is generally~~ and often water proof (Wu and Zhang, 2008; Song et al., 2015; Lin et al., 2015). The water thawed during the day time would freeze again at night on the soil surface (Supplementary Figure 10~~:~~a; Shi et al., 2006; Wu and Zhang, 2010b). The thin-ice layer could stop atmospheric gases of CH_4 and O_2 from getting into the soils (Gazovic et al., 2010). During ~~autumn~~ autumn, the SWC ~~of 10cm~~ is 15.3%~~,~~ at 10 cm below ground, decreases to 9.4% at 20-40 cm, and then increases to 13.6% and 21.0% at ~~20-40cm is only 9.4%, but~~ 80 cm ~~is 13.6%,~~ and 160 cm, respectively ~~can up to 21.0%~~ (Supplementary Table 1).~~,~~ ~~however~~However, soils are bi-directionally frozen from both top (ground surface) and bottom~~, the~~ (permafrost table~~,~~) which is about 200~400 cm ~~deep~~ below ground~~;~~ (Supplementary Figure 8; ~~Wu and Zhang, 2010a),~~ Wu and Zhang, 2010a). ~~doesn't form a layer of thin ice during the nighttime surface soil freezing, because o~~On the one hand, the frozen soil of the ground surface (about 0-40cm) prevents the outside liquid water from permeating. On the other hand, the freezing itself will reduce the liquid water content in the soil. ~~(Ma et al., 2015)~~ Therefore, it creates finely closed anaerobic gaps that allow CH_4 and O_2 gases into deep soils (about 50~400 cm; Mastepanov et al., 2008; Mastepanov et al., 2013; Zona et al., 2016). Meanwhile, the temperature of deep soils (about 50~400 cm)~~,~~ still remains at a relatively high level (Supplementary Figure 10~~:~~b), and methanotrophic bacteria ~~there are~~ will still be active at this high T_{soil} (Figure 2). This could be one important mechanism for ~~autumn~~ autumn soil CH_4 consumption. In addition, in principal it ~~was~~ is also possible that the observed seasonal variation in CH_4 flux may actually arise from the spatial variation of the footprint covered by the

Formatted: Highlight
Formatted: Highlight
Formatted: Highlight
Formatted: Highlight
Formatted: Highlight
Formatted: Highlight
Formatted: Highlight
Formatted: Highlight
Formatted: Highlight
Formatted: Highlight
Formatted: Highlight
Formatted: Highlight
Formatted: Highlight
Formatted: Highlight
Formatted: Highlight
Formatted: Highlight
Formatted: Subscript

eddy covariance site (within 175 m), given that prevalent wind direction changes seasonally (Supplementary Figure 4). Nonetheless, we found that the same vegetation species and soil exist in different directions to the tower within the footprint (Supplementary Figure 11). ~~Hence t~~This spatial vegetation and soil homogeneity rules out the potential influence of footprint changes on the sign of CH_4 balances, and further confirms that seasonal soil freezing and thawing differences may likely be the main explanation for seasonal CH_4 variations.

Furthermore, we suggested that the specific ~~autumn~~ autumn soil vertical structure may help to explain why the site was a CH_4 sink, unlike the CH_4 source in ~~spring~~ spring. The sequential probing data enables us to establish a rough estimate on the soil vertical structure during the ~~autumn~~ autumn thawing–freezing process, in which the vertical distribution of clay, sandy soils, and soil organic layers was mixed like a multi–layer hamburger structure, rather than forming a gradual change (Figure 6~~:~~ e). As the soil profile is vertically ~~has a~~ different in features such as soil density, thermal conductivity, latent heat ~~of phase transition~~, soil salinity, ~~of soil, and so on~~ etc., we boldly conjecture that ~~, similarly,~~ the T_{soil}, SWC, and soil microbial activities also had this hamburger type of vertical distribution in a similar way. As a result, layers of frozen and thawed soils were not changing gradually but appeared like a hamburger structure too. This ~~hamburger–like~~ soil vertical structure trapped high concentrations of soil water between the frozen layers, which was therefore highly anaerobic and suitable for CH_4 production. It may also allow ~~Also, because of the hamburger–like structure, it fueled~~ speculation that biogenic CH_4 between frozen layers could not escape in ~~autumn~~ autumn. The biogenic CH_4 ~~was~~ would be trapped until the ~~ACL~~ active soil layer was completely frozen in late ~~autumn~~ autumn, and in some warmer years until early ~~winter~~ winter and created frost cracks. This would enable~~d~~ it to escape and may explain why there was a large burst of CH_4 emissions in late ~~autumn~~ autumn

Formatted: Subscript

Formatted: Subscript

and early ~~winter~~ winter and may also explain the constantly weak CH_4 emission through the ~~winter~~ winter season, although methanogenic bacteria may have stopped functioning in the low temperature of ~~winter~~ winter. Of course, ~~this will need~~ further ~~study~~ studies and direct data collection in the field will be needed to fully test the hypothesis ~~and necessitates direct data collection in the field~~.

4.2 Impacts of Environmental, Permafrost, and Microbial Activities on CH_4 Fluxes

Our results demonstrated the important roles of climate, freezing and thawing dynamics, and soil microbe activities in regulating the direction and amount of CH_4 exchanges between the atmosphere and ecosystems in permafrost areas. The key role of the above factors and processes was also confirmed by the better representation of seasonal CH_4 cycles by our new seasonal division method based on soil microbes, temperature, and permafrost dynamics rather than T_{air} or vegetation phenology. Here, we further discuss potential mechanisms of how environmental (including air and soil heat and water), freezing and thawing processes, and soil microbes control the production and absorption of CH_4.

First, it is noteworthy that both the strength and direction of correlations between CH_4 fluxes, SWC, and T_{soil} parameters changed with soil depths, particularly during ~~spring~~ spring and ~~autumn~~ autumn, when active layer soils shifted between thawing and freezing regularly. The positive and negative CH_4 flux correlations with T_{soil} ~~($p<0.01$)~~ and SWC ~~($p<0.01$)~~ may suggest that the impacts of T_{soil} and SWC on CH_4 fluxes shall be treated as a holistic process (Table 3), rather than as separate ones. For instance, in ~~autumn~~ autumn, the significant correlation between CH_4 fluxes and T_{soil} ~~($p<0.01$)~~ or SWC ~~($p<0.01$)~~ was positive at some soil depths, but negative at some other depths, reaching the maximum at the depth of 80 cm. Further, *in situ* observations suggested that soil organic matter and soil microbe amount were also at a very high level at this

Formatted: Subscript

Formatted: Subscript

Formatted: Subscript

Formatted: Subscript

Formatted: Subscript

depth, highlighting that the regulation of soil abiotic factors on CH_4 cycling may be well influenced by soil biotic activities. In addition, the holistic soil heat–water process could also determine the concentration of soil inorganic ions, particularly during ~~spring~~ spring and ~~autumn~~ autumn, which were critical factors controlling the amount of soil unfrozen water. Earlier studies suggested that ~~S~~soil unfrozen water ~~in winter~~ is ~~perhaps being~~ important for maintaining soil microbial activities in winter (Panikov and Dedysh, 2000~~; Rivkina et al., 2004);~~; Rivkina et al., 2004). ~~and i~~In the future ~~work~~ we will include data acquiring of soil unfrozen water ~~and~~ to test its role in regulating CH_4 exchanges in permafrost regions.

T_{air} and precipitation impact CH_4 fluxes indirectly through their influences on T_{soil} and SWC (Zhuang et al., 2004; Lecher et al., 2015). Such indirect influences may often be characterized with time–lagged effects (Koven et al., 2011). For instance, post–drought rainfall events in ~~summer~~ summer can first promote soil CH_4 consumption (~~summer~~ summer of 2014). This is because certain soil moisture is needed for methanogenic bacteria to function (Del et al., 2000; Luo et al., 2012). Yet, prolonged rainfall will eventually cause CH_4 fluxes to change from negative (soils consume CH_4) to positive (soils emit CH_4) fluxes (for example, day 168th to 183th of 2015, Figure 3~~:~~ d). After rainfall events, CH_4 flux gradually turned negative again with the decrease of SWC. As a result of these time–lagged effects, the correlation coefficient between CH_4 fluxes and precipitation often appears very low, although still statistically significant.

Second, soil methanogenic and methanotrophic bacteria could co–exist with different optimal niches (e.g., ranges of T_{air} / T_{soil} and SWC; Zhuang et al., 2013; Lau et al., 2015; Wei et al., 2015a). For example, the CH_4 ~~diel~~d~~iurna~~iel cycle in ~~summer~~ summer was found to have two strong consumption peaks and one weak emission peak (Figure 4: a3, c3, d3, e3). The timing of these different peaks may well reflect the different environmental requirements for the

Formatted: Highlight
Formatted: Highlight
Formatted: Highlight
Formatted: Highlight
Formatted: Highlight
Formatted: Highlight
Formatted: Highlight
Formatted: Highlight
Formatted: Highlight
Formatted: Highlight
Formatted: Subscript
Formatted: Subscript
Formatted: Subscript
Formatted: Subscript

dominance of methanogens and methanotrophic bacteria. Furthermore, methanogens may have a broader functional temperature range than methanotrophic bacteria (Kolb, 2009; Lau et al., 2015; Yang et al., 2016). This is also evident, for example, from the dieldiurnaiel CH_4 cycle in autumn autumn when CH_4 consumption was minimal at both lowest and highest T_{air} (Figure 4; a4, b4, c4, d4, 4 e4).

The complex relationships between CH_4 fluxes and environmental factors make it a grand challenge to predict the future of the QTP CH_4 budget under a changing climate. For instance, it has been generally believed that the ALT will increase under projected warming (Wu and Liu, 2004). The positive correlation between CH_4 fluxes and ALT found here suggests that the QTP permafrost CH_4 sink may thus be weakened. However, the negative correlation between CH_4 flux and T_{air} may lead to a different conclusion. Incorporating our findings and high–resolution data into mechanistic CH_4 models is therefore needed to enhance our capacity in predicting future CH_4 budgets. Earth system models have been introduced to estimate CH_4 dynamics (Curry, 2007; Spahni et al., 2011; Bohn et al., 2015). For example, using a terrestrial ecosystem modelling approach, Zhuang et al. (2004) estimated the average QTP permafrost CH_4 sink of -0.08 g C m^{-2} yr^{-1}, much smaller than our field–based CH_4 estimate (-0.86 ± 0.23 g CH_4–C m^{-2} yr^{-1}). Current CH_4 models focus on the regulation of CH_4 processes by temperature and SWC, and usually lack high–resolution data for model parameterization (Bohn et al., 2015). Data interpolation and the use of average values of certain environmental factors are normal practices in most models (Zhuang et al., 2004), which may overlook the impacts of environmental variations on CH_4 dynamics. For example, at Beilu'he, T_{air} on a typical summer day (e.g., July 6th, 2013) could vary between -6 °C and 28 °C, a difference of 34 °C. The resulting dieldiurnaiel mean temperature, 17 °C, is beyond the range of methanotrophic bacteria's preferable

Formatted: Subscript

Formatted: Subscript

Formatted: Subscript

temperature of 20～30 °C (Segers, 1998; Steinkamp et al., 2001; Yang et al., 2016). Therefore, models using ~~diel~~d~~iurna~~iel mean temperature as an input may estimate the site as a net CH_4 sink. However, field observations show a source with a sink only during a short period (8:30am～11:30 am), on July 6th, 2013, because the short period of the sink was offset by the source over the remaining 21 hours.

Furthermore, half–hourly SWC was well related with the waterproof role by the permafrost layer during ~~spring~~ spring and ~~autumn~~ autumn (Figure 6~~:~~ a). However, because of the shortage of high temporal resolution data, half–~~diel~~di~~urna~~el or ~~diel~~di~~urna~~el mean SWC data are often used in many previous studies (Zhu et al., 2004; Jiang et al., 2010; Wei et al., 2015b), which could not correctly show the regulation of permafrost soil properties that are critical for CH_4 dynamics. As another example, T_{soil} of 0 − 50 cm depth is one of the most important factors related to CH_4 fluxes (Mastepanov et al., 2008). However, many studies used T_{air} or re–analyzed deep T_{soil} instead (Zhu et al., 2004; Bohn et al., 2015; Oh et al., 2016). Because the active layer is not homogeneous, but with different thermal conductivities during the freezing and thawing process, the use of T_{air} or deep T_{soil} brings in large uncertainties in CH_4 modelling. Future research needs to improve mechanistic understanding of CH_4 dynamics and their biotic and abiotic control factors, and to conduct more high–resolution and long–term field monitoring.

4.3 The Classification System of the Four Seasons for CH_4 Studies

Our study ~~is also different~~ differs also from the majority of earlier studies regarding the definition of the seasons~~in seasonal definitions~~ (Treat et al., 2014; Wang et al., 2014; Wei et al., 2015a; Song et al., 2015). Here, we adopted a new classification system of the four seasons based on 0 − 25 cm soil depth bacterial activities (Figure 2), T_{soil} of 0 − 40 cm (Supplementary Figure 6~~:~~ a), and ALT (Supplementary Figure 8), rather than the conventional methods based on

Formatted: Subscript
Formatted: Subscript
Formatted: Subscript
Formatted: Subscript
Formatted: Subscript
Formatted: Font color: Auto
Formatted: Font color: Auto
Formatted: Subscript

T_{air} and vegetation dynamics (Chen et al., 2011; McGuire et al., 2012). Previous studies indicated that changes in CH_4 fluxes are regulated by soil microbes, and activities of soil microbes are not limited to the warm season (Zhuang et al., 2004; Lau et al., 2015; Yang et al., 2016). For instance, in March and November, we found the amount of gene expression by methanogens and methanotrophs at 0 − 25 cm soils were about 16.8% and 35.6% (Figure 2), respectively, suggesting there are still strong microbial activities during the cold and dry season. Therefore, our new method of defining the four seasons from the top soil's biotic and abiotic features better captures the pattern of CH_4 dynamics throughout a year.

Formatted: Subscript

5. Conclusions

Our field data indicates that there was a large CH_4 sink in the QTP permafrost area during recent years. The strength of this CH_4 sink is larger than found in previous studies in the same region and many high–latitude tundra ecosystems. This study highlights the complexity of environmental controls, including soil heat–water processes, permafrost freezing and thawing dynamics, and soil microbial activities, on CH_4 cycling. This complexity implies that linear interpolation and extrapolation from site-level studies could introduce large uncertainties in CH_4 flux estimation. Future quantification of CH_4 dynamics in permafrost regions needs to account for the effects of complex environmental processes, including freezing and thawing, and the interaction between heat and water, as well as microbial activities. Our findings also highlight the importance of conducting more high–resolution and long–term field monitoring in permafrost regions for better understanding and modelling of permafrost CH_4 cycling under a changing climate.

Acknowledgements

We would like to thank Yongzhi Liu, Jing Luo, Ji Chen, Guilong Wu, Wanan Zhu, Zhipeng Xiao, and Chang Liao for their tremendous help in collecting field data over all these years. We also want to pay tribute and gratitude to the late Xiaowen Cui for his contribution to our many field adventures. We thank John McCabe for proofreading the manuscript. This study was supported by the National Natural Science Foundation of China (41501083), Key Research Program of Frontier Sciences, Chinese Academy of Sciences (QYZDJ-SSW-DQC011), Opening Research Foundation of Key Laboratory of Land Surface Process and Climate Change in Cold and Arid Regions, Chinese Academy of Sciences (LPCC201307), and Opening Research Foundation of Plateau Atmosphere and Environment Key Laboratory of Sichuan Province (PAEKL − 2014 − C3). A. C. acknowledges the support from a Purdue University Forestry and Natural Resources research scholarship. The data generated in this study will be freely available on the Asia Flux regional network server (https://db.cger.nies.go.jp/asiafluxdb/).

Reference

Bohn T., Melton J., Ito A.: WETCHIMP–WSL: intercomparison of wetland methane emissions models over West Siberia, Biogeosciences, 12, 3321 – 3349, 2015.

Burba, G. G., Mcdermitt, D. K., and Grelle, A.: Addressing the influence of instrument surface heat exchange on the measurements of CO_2 flux from open–path gas analyzers. Glob. Change Biol., 14(8), 1854 – 1876, 2008.

Cao G., Xu X., and Long R.: Methane emissions by alpine plant communities in the Qinghai–Tibet Plateau, Biol. Lett., 4, 681 – 684, 2008.

Cao B., Gruber S., Zhang T.: Spatial variability of active layer thickness detected by ground–

penetrating radar in the Qilian Mountains, Western China, J. Geophys. Res. Earth Surf., 122, 574 – 591, 2017.

Cate, R. B., and Nelson, L. A.: A simple statistical procedure for partitioning soil test correlation data into two classes, Soil Sci. Soc. Am. J., 35(4), 658 – 660, 1971.

Chang R., Miller C., and Dinardo S.: Methane emissions from Alaska in 2012 from CARVE airborne observations, Proc. Natl. Acad. Sci. U. S. A., 111, 16694 – 16699, 2014.

Chang S. and Shi P.: A review of research on responses of leaf traits to climate change, Chin. J. Plant Ecol., 39, 206 – 216, 2015.

Chen W., Wolf B., and Zheng X.: Annual methane uptake by temperate semiarid steppes as regulated by stocking rates, aboveground plant biomass and topsoil air permeability. Glob. Change Biol., 17, 2803 – 2816, 2011.

Curry C.: Modeling the soil consumption at atmospheric methane at the global scale. Glob. Biogeochem. Cycles, 21, 1 – 15, 2007.

Dengel S., Zona D., and Sachs T.: Testing the applicability of neural networks as a gap–filling method using CH_4 flux data from high latitude wetlands. Biogeosciences, 10, 8185 – 8200, 2013.

Del G., Parton W., and Mosier A.R.: General CH_4 oxidation model and comparisons of CH_4 oxidation in natural and managed systems, Glob. Biogeochem. Cycles, 14, 999 – 1019, 2000.

Falge, E., Baldocchi, D., and Olson, R.: Gap filling strategies for defensible annual sums of net ecosystem exchange, Agric. For. Meteorol., 107(1), 43 – 69, 2001.

Gažovič M., Kutzbach L., and Schreiber P.: Diurnal dynamics of CH_4 from a boreal peatland during snowmelt. Tellus, B, 62, 133 – 139, 2010.

IPCC, climate change 2013: the physical science basis. Contribution of working group I to the fifth assessment report of the intergovernmental panel on climate change., 2013.

Jansson, J. K. and Tas, N.: The microbial ecology of permafrost, Nat. Rev. Microbiol., 12, 414, 2014.

Jiang C., Yu G., and Fang H.: Short–term effect of increasing nitrogen deposition on CO_2, CH_4 and N_2O fluxes in an alpine meadow on the Qinghai–Tibetan Plateau, China, Atmos. Environ., 44, 2920 – 2926, 2010.

Jin H., Li S., and Cheng G.: Permafrost and climatic change in China, Glob. Planet, Change, 26, 387 – 404, 2000.

Jørgensen, C. J., Johansen, K. M. L., and Westergaard–Nielsen, A.: Net regional methane sink in High Arctic soils of northeast Greenland, Nat. Geosci., 8, 20, 2015.

Kirschke, S., Bousquet, P., and Ciais, P.: Three decades of global methane sources and sinks, Nat. Geosci., 6, 813, 2013.

Kolb, S.: The quest for atmospheric methane oxidizers in forest soils, Environ. Microbiol. Rep., 1, 336 – 346, 2009

Koven C.D., Ringeval B., and Friedlingstein P.: Permafrost carbon–climate feedbacks accelerate global warming, Proc. Natl. Acad. Sci. U. S. A., 108, 14769 – 14774, 2011.

Lau M., Stackhouse B.T., and Layton A.C.: An active atmospheric methane sink in high Arctic mineral cryosols. ISME J., 9, 1880 – 1891, 2015.

Lecher A.L., Dimova N., and Sparrow K.J.: Methane transport from the active layer to lakes in the Arctic using Toolik Lake, Alaska, as a case study, Proc. Natl. Acad. Sci. U. S. A., 112, 3636 – 3640, 2015.

Lee, X., Massman, W., and Law, B. (Eds.): Handbook of micrometeorology: a guide for surface flux measurement and analysis (Vol. 29), Springer Science and Business Media, 2006.

Li K., Gong Y., and Song W.: Responses of CH_4, CO_2 and N_2O fluxes to increasing nitrogen deposition in alpine grassland of the Tianshan Mountains, Chemosphere, 88, 140 – 143, 2012.

Liebner S., Zeyer J., and Wagner D.: Methane oxidation associated with submerged brown mosses reduces methane emissions from Siberian polygonal tundra, J. Ecol., 99, 914 – 922, 2011.

Lin Z., Burn C.R., and Niu F.: The Thermal Regime, including a Reversed Thermal Offset, of Arid Permafrost Sites with Variations in Vegetation Cover Density, Wudaoliang Basin, Qinghai–Tibet Plateau. Permafr. Periglac. Process., 26, 142 – 159, 2015.

Loescher, H. W., Law, B. E., and Mahrt, L: Uncertainties in, and interpretation of, carbon flux estimates using the eddy covariance technique. J. Geophys. Res. Atmos., 111(D21), 2006.

Luo G.J., Brüggemann N., and Wolf B.: Decadal variability of soil CO_2, NO, N_2O, and CH_4 fluxes at the Höglwald Forest, Germany. Biogeosciences, 9, 1741 – 1763, 2012.

Mastepanov M., Sigsgaard C., and Dlugokencky E.J.: Large tundra methane burst during onset of freezing. Nature, 456, 628 – 30, 2008.

Mastepanov, M., Sigsgaard, C., and Tagesson, T.: Revisiting factors controlling methane emissions from high-Arctic tundra, Biogeosciences, 10(7), 5139, 2013.

~~Ma W., Zhang L., and Yang C.: Discussion of the applicability of the generalized Clausius–Clapeyron equation and the frozen fringe process, Earth-Sci. Rev., 142, 47-59, 2015.~~

Mauder, M., Cuntz, M., and Drüe, C.: A strategy for quality and uncertainty assessment of long–term eddy–covariance measurements. Agric. For. Meteorol., 169, 122 – 135, 2013.

McGuire A.D., Christensen T.R., and Hayes D.: An assessment of the carbon balance of Arctic tundra: Comparisons among observations, process models, and atmospheric inversions, Biogeosciences, 9, 3185 – 3204, 2012.

Moncrieff, J., Clement, R., and Finnigan, J.: Averaging, detrending, and filtering of eddy covariance time series. In Handbook of micrometeorology (pp. 7 – 31), Springer Netherlands, 2004.

Muller, S. W. Permafrost or permanently frozen ground and related engineering problems, 1947.

Oh Y., Stackhouse B., and Lau M.: A scalable model for methane consumption in arctic mineral soils. Geophys. Res. Lett., 43, 5143 – 5150, 2016.

Panikov N.S. and Dedysh S.N.: Cold season CH_4 and CO_2 emission from boreal peat bogs (West Siberia): Winter fluxes and thaw activation dynamics, Glob. Biogeochem. Cycles, 14, 1071 – 1080, 2000.

Papale, D., Reichstein, M., and Aubinet, M.: Towards a standardized processing of Net Ecosystem Exchange measured with eddy covariance technique: algorithms and uncertainty estimation. Biogeosciences, 3(4), 571 – 583, 2006.

Patra P.K. and Kort E.A.:Regional Methane Emission Estimation Based on Observed

Formatted: Indent: Left: 0 cm, First line: 0 cm

Atmospheric Concentrations (2002 – 2012), J. Meteor. Soc. Japan. Ser. II, 94, 91 – 113, 2016.

Qin, Y., Wu T., and Li R., Using ERA-Interim reanalysis dataset to assess the changes of ground surface freezing and thawing condition on the Qinghai–Tibet Plateau. Environ. Earth Sci., 75(9): 1-13, 2016.

Rigby M., Prinn R.G., and Fraser P.J.: Renewed growth of atmospheric methane, Geophys. Res. Lett.,35, 2 – 7, 2008.

Rivkina E., Laurinavichius K., and McGrath J.: Microbial life in permafrost, Adv. Space Res., 33, 1215 – 1221, 2004.

Segers R.: Methane production and methane consumptiona–review of processes underlying wetland methane fluxes [Review], Biogeochem., 41, 23 – 51, 1998.

Shi P., Sun X., and Xu L.: Net ecosystem CO_2 exchange and controlling factors in a steppe–Kobresia meadow on the Tibetan Plateau. Sci. China Ser. D-Earth Sci., 49, 207 – 218, 2006.

Song, W., Wang, H., and Wang, G.: Methane emissions from an alpine wetland on the Tibetan Plateau: Neglected but vital contribution of the non–growing season, J. Geophys. Res. Biogeosci., 120, 1475 – 1490, 2015.

Spahni R., Wania R., and Neef L.: Constraining global methane emissions and uptake by ecosystems. Biogeosciences, 8, 1643 – 1665, 2011.

Steinkamp R., Butterbach–Bahl K., and Papen H.: Methane oxidation by soils of an N limited and N fertilized spruce forest in the Black Forest, Germany, Soil. Biol. Biochem., 33, 145 – 153, 2001.

Sturtevant C.S., Oechel W.C., and Zona D.: Soil moisture control over autumn season methane flux, Arctic Coastal Plain of Alaska, Biogeosciences, 9, 1423 – 1440, 2012.

Treat C.C., Wollheim W.M., and Varner R.K.: Temperature and peat type control CO_2 and CH_4 production in Alaskan permafrost peats, Glob. Chang. Biol. 20, 2674 – 2686, 2014.

Vickers, D., and Mahrt, L.: Quality control and flux sampling problems for tower and aircraft data. J. Atmos. Ocean. Technol., 14(3), 512 – 526, 1997.

Wang G., Li Y., and Wang Y.: Effects of permafrost thawing on vegetation and soil carbon pool losses on the Qinghai–Tibet Plateau, China, Geoderma, 143, 143 – 152, 2008.

Wang S., Jin H., Li S.: Permafrost degradation on the Qinghai–Tibet Plateau and its environmental impacts. Permafr. Periglac. Process., 11, 43 – 53, 2000.

Wang Y., Liu H., and Chung H.: Non–growing season soil respiration is controlled by freezing and thawing processes in the summer monsoon-dominated Tibetan alpine grassland. Glob. Biogeochem. Cycles, 28, 1081 – 1095, 2014.

Webb~~,~~ E. K., ~~G. I.~~ Pearman G. I., and ~~R.~~ Leuning R.: Correction of flux measurements for density effects due to heat and water vapor transfer. Q. J. Royal Meteorol. Soc., 106, 85 – 100, 1980.

Wei D., Ri X., and Wang Y.: Responses of CO_2, CH_4 and N_2O fluxes to livestock exclosure in an alpine steppe on the Tibetan Plateau, China. Plant Soil, 359, 45 – 55, 2012.

Wei D., Ri X., and Tarchen T.: Considerable methane uptake by alpine grasslands despite the cold climate: In situ measurements on the central Tibetan Plateau, 2008 – 2013, Glob. Chang Biol., 21, 777 – 788, 2015a.

Wei D., Tarchen T., and Dai D.: Revisiting the role of CH_4 emissions from alpine wetlands on

Formatted: Default Paragraph Font, Font: (Default) +Body (Calibri), 11 pt, Check spelling and grammar

Formatted: Default Paragraph Font, Font: (Default) +Body (Calibri), 11 pt, Check spelling and grammar

Formatted: Default Paragraph Font, Font: (Default) +Body (Calibri), 11 pt, Check spelling and grammar

Formatted: Font: Not Italic

Formatted: Default Paragraph Font, Font: (Default) +Body (Calibri), 11 pt, Check spelling and grammar

Formatted: Default Paragraph Font, Font: (Default) +Body (Calibri), 11 pt, Check spelling and grammar

Formatted: Default Paragraph Font, Font: (Default) +Body (Calibri), 11 pt, Check spelling and grammar

Formatted: Default Paragraph Font, Font: (Default) +Body (Calibri), 11 pt, Check spelling and grammar

Formatted: Font: (Default) Times New Roman, 12 pt, Do not check spelling or grammar

the Tibetan Plateau: Evidence from two in situ measurements at 4758 and 4320 m above sea level, J. Geophys. Res. Biogeosci., 120, 1741 – 1750, 2015b.

Whalen, S. C. and Reeburgh, W. S.: Consumption of atmospheric methane by tundra soils. Nature, 346, 160, 1990.

Whalen S.C.: Biogeochemistry of Methane Exchange between Natural Wetlands and the Atmosphere. Environ. Eng. Sci., 22, 73 – 94, 2005.

Whalen S.C., Reeburgh W.S., and Barber V.A.: Oxidation of methane in boreal forest soils: a comparison of seven measures. Biogeochemistry, 16, 181 – 211, 1992.

Wilson K., et al.: Energy balance closure at FLUXNET sites. Agr Forest Meteorol., 113: 223-243, 2002.

Wu Q. and Liu Y.: Ground temperature monitoring and its recent change in Qinghai–Tibet Plateau, Cold Reg. Sci. Technol., 38, 85 – 92, 2004.

Wu Q. and Zhang T.: Recent permafrost warming on the Qinghai–Tibetan Plateau. J. Geophys. Res. Atmos. 113, 1 – 22, 2008.

Wu Q.and Zhang T.: Changes in active layer thickness over the Qinghai–Tibetan Plateau from 1995 to 2007, J. Geophys. Res. Atmos., 115, D09107, 2010a.

Wu Q. Zhang T., and Liu Y.: Permafrost temperatures and thickness on the Qinghai–Tibet Plateau, Glob. Planet. Change, 72, 32 – 38, 2010b.

Yang S., Wen X., and Shi Y.: Hydrocarbon degraders establish at the costs of microbial richness, abundance and keystone taxa after crude oil contamination in permafrost environments. Sci. Rep., 6, 37473, 2016.

Zhu X., Zhuang Q., and Chen M.: Net exchanges of methane and carbon dioxide on the Qinghai–Tibetan Plateau from 1979 to 2100. Environ. Res. Lett., 10, 85007. 2004.

Zhuang Q., Melillo J.M., and Kicklighter D.W.: Methane fluxes between terrestrial ecosystems and the atmosphere at northern high latitudes during the past century: A retrospective analysis with a process–based biogeochemistry model. Glob. Biogeochem. Cycles, 18(3), 2004.

Zhuang Q., Chen M., and Xu K.: Response of global soil consumption of atmospheric methane to changes in atmospheric climate and nitrogen deposition. Glob. Biogeochem. Cycles, 27, 650 – 663, 2013.

Zona D., Gioli B., and Commane R.: Cold season emissions dominate the Arctic tundra methane budget. Proc. Natl. Acad. Sci. U. S. A., 113, 40 – 45, 2016.

Table 1. Soil characteristics at the eddy covariance flux study site

Soil depth	Soil type	Gravel content	SOC	Microbial Numbers	pH	DBD	SWC	Total N
cm		g kg^{-1}	g kg^{-1}	$\times 10^4$		g cm^{-3}	%	$\times 10^3$ mg kg^{-1}
0 – 20	clay	22.3	2.8	3.44	8.7	1.75	18.26	0.87
20 – 50	~~Silty~~ silty clay	12.6	1.7	3.82	8.4	1.73	11.52	1.02
50 – 120	silt and fine sand	3.4	1.3	3.67	8.4	1.72	12.57	1.18
120 – 160	silt and fine sand	2.8	26.4	5.44	5.1	1.68	24.69	2.46
160 – 200	silt and fine sand	1.6	13.6	4.39	6.8	1.68	22.45	2.03

Note: Gravel content diameter ≥ 0.5cm. SOC is soil organic content, DBD is dry bulk density, ~~and~~ SWC is soil water content, and Total N is total nitrogen content.

Table 2. Measurements of four seasons from 2012 to 2016

	Spring	Summer	Autumn	Winter	Plant growing season	Plant non–growing season
	Period; Total days	Period; Total days	Period; Total days	Period; Total days	Period; Total days	Period; Total days
	Days	Days	Days	Days	Days	Days
2012	50 – 142; 93	143 – 229; 87	230 – 323; 94	1 – 49, 324 – 366; 92	139 – 286; 148[a]	1 – 138, 287 – 366; 218[a]
					122 – 305; 184[b]	1 – 121, 306 – 366; 182[b]
					143 – 290; 148[c]	1 – 142, 291 – 366; 218[c]
2013	36 – 137; 102	138 – 224; 87	225 – 334; 110	1 – 35, 335 – 365; 66	139 – 287; 149[a]	1 – 138, 288 – 365; 216[a]
					121 – 304; 184[b]	1 – 120, 305 – 365; 181[b]
					127 – 297; 171[c]	1 – 126, 298 – 365; 194[c]
2014	49 – 127; 79	128 – 228; 101	229 – 309; 81	1 – 48, 310 – 365; 104	137 – 288; 152[a]	1 – 136, 289 – 365; 213[a]
					121 – 304; 184[b]	1 – 120, 305 – 365; 181[b]
					142 – 294; 153[c]	1 – 141, 295 – 365; 212[c]
2015	36 – 150; 115	151 – 224; 74	225 – 312; 88	1 – 35, 313 – 365; 88	145 – 288; 144[a]	1 – 144, 289 – 365; 221[a]
					121 – 304; 184[b]	1 – 120, 305 – 365; 181[b]
					136 – 295; 160[c]	1 – 135, 296 – 365; 205[c]
2016	47 – 161; 115	162 – 225; 64	226 – 299; 74	1 – 46, 300 – 366; 113	141 – 287; 147[a]	1 – 140, 288 – 366; 219[a]
					122 – 305; 183[b]	1 – 120, 305 – 366; 182[b]
					140 – 296; 157[c]	1 – 139, 297 – 366; 209[c]

Note: [a], based on vegetation cover and temperature change (VCT) (Lund et al., 2010; Tang and Arnone, 2013; Song et al., 2015); [b], based on Julian months (JMC) (Da et al., 2015); [c], based on vegetation phenology change (VPC). ~~Spring~~ Spring , ~~Summer~~ Summer, ~~Autumn~~ Autumn, ~~Winter~~ Winter are based on parameters of microbial activities, ALT variety coefficient and T_{soil} (SMT).

Formatted: Subscript

Table 3. Correlation coefficients between CH_4 fluxes and environment factors on half–hour time scales

Environment Factors	~~Spring~~ Spring		~~Summer~~ Summer		~~Fall~~ Autumn		~~Winter~~ Winter		2012 – 2016	
	CH_4 Flux									
	r	n	r	n	r	n	r	n	r	n
T_{air}	0.25**	24144	0.14**	19818	-0.16**	20959	0.32**	22224	-0.11**	87145
Wind Speed	0.31**	24144	-0.04**	19817	-0.20**	20959	0.32**	22224	0.15**	87144
VPD	-0.33**	18624	-0.21**	19263	-0.09**	16737	-0.21	18000	0.26**	69624
Rn	0.55**	24143	0.09**	19807	-0.33**	20913	0.51**	22224	0.09**	87087
Albedo	0.07**	24144	-0.01	19814	-0.08**	20913	0.10**	22224	0.02**	87095
SHF of 5cm	0.46**	24144	-0.08**	19818	-0.23**	20913	0.43**	22224	0.09**	87099
SHF of 15cm	0.36**	24144	-0.15**	19815	-0.23**	20913	0.33**	22224	0.08**	87096
SWC of 10cm	-0.16**	24144	-0.14**	19818	-0.06**	20959	0.00	22224	-0.25**	87145
SWC of 20cm	-0.15**	24144	-0.13**	19816	-0.07**	20959	0.11**	22224	-0.24**	87143
SWC of 40cm	-0.11**	24144	-0.02**	19818	0.07**	20959	0.06**	22224	-0.17**	87145
SWC of 80cm			-0.13**	19818	0.06**	20959				
SWC of 160cm			0.04**	19818	-0.11**	20959				
Precipitation			-0.02	16748	0.01[b]	17888				
ALT	0.73**	23004	0.23**	19823	0.73**	21454			0.43**	64281

Formatted: Subscript

ΔI	0.77^{**}	100	0.57^{**}	83	0.46^{**}	89	0.23	93	0.49^{**}	365
ΔII	0.31^{**}	100	0.66^{**}	83	0.78^{**}	89	0.19	93	0.52^{**}	365
T_{soil} of 0 cm	-0.06^{*}	23004	0.13^{**}	19823	0.07^{**}	20366	0.13^{**}	21711	0.11^{**}	84904
T_{soil} of 5 cm	0.15^{**}	24144	0.15^{**}	19808	-0.13^{**}	21454	0.27^{**}	22224	0.24^{**}	87630
T_{soil} of 10 cm	-0.03^{**}	24144	0.12^{**}	19808	0.08^{**}	21454	0.16^{**}	22224	0.13^{**}	87630
T_{soil} of 20 cm	-0.14^{**}	24144	0.08^{**}	19808	0.02^{**}	21454	0.06^{**}	22224	-0.09^{**}	87630
T_{soil} of 30 cm	-0.13^{**}	23004	0.06^{**}	19823	-0.02^{**}	20366	0.07^{**}	21711	-0.08^{**}	84904
T_{soil} of 40 cm	0.14^{**}	24144	0.05^{**}	19808	-0.01^{b}	21454	0.06^{**}	22224	0.11^{**}	87630
T_{soil} of 50 cm			0.04^{**}	19823	-0.05^{**}	20366				
T_{soil} of 70 cm			0.07^{**}	19823	-0.05^{**}	20366				
T_{soil} of 80 cm			0.05^{**}	19808	0.04^{**}	21454				
T_{soil} of 100 cm			0.10^{**}	19823	-0.05^{**}	21454				
T_{soil} of 150 cm			0.09^{**}	19823	-0.04^{**}	20366				
T_{soil} of 160 cm			0.10^{**}	19808	0.01^{**}	21454				
T_{soil} of 200 cm			0.02^{**}	19823	-0.02^{**}	20366				

Note: ** means p<0.01, * means p<0.05; r values for the relationship between CH_4 flux and environment factors. T_{air} means air temperature of 3 m above the ground surface. VPD is vapor pressure deficit, NR is net radiation, and SWC is soil water content, ALT is active layer thickness, which fitted through the depth of soil 0 □ in Surfer 8.0., and the data is removed as meaningless in winter. T_{soil} is the temperature of the soil. In

Formatted: Subscript

Formatted: Subscript

spring spring and winter winter, precipitation data is too sparse for statistical analysis. ΔI is the soil 0 − 25cm archaeal methanogens gene expression, and ΔⅡ is the soil 0− 25 cm methanotrophic gene expression. The coefficients (r) between CH_4 flux and ΔI, ΔⅡ are obtained using the synchronous CH_4 fluxes averaged for 5 days.

Table 4. Principal components analysis (PCA) of the environmental factors.

	~~Spring~~ Spring				~~Summer~~ Summer				~~autumn~~ aAutumn				~~Winter~~ Winter			
Component	PC1	PC2	PC3	PC4	PC1	PC2	PC3	PC4	PC1	PC2	PC3	PC4	PC1	PC2	PC3	PC4
wind speed	-0.03	0.51	0.65	-0.46	0.02	0.37	0.38	-0.13	-0.04	0.44	0.59	0.67	0.27	0.45	-0.11	-0.27
T_{air}	0.38	0.29	-0.05	-0.11	0.42	0.22	-0.03	0.02	0.36	0.21	0.08	-0.06	0.48	0.12	-0.02	0.01
VPD	0.34	-0.27	0.40	0.15	0.17	0.46	-0.22	0.09	0.34	-0.15	0.17	-0.07	0.14	-0.15	0.95	-0.22
Rn	0.16	0.49	0.00	0.76	-0.01	0.07	0.58	0.11	0.12	0.54	-0.43	-0.07	0.26	0.47	-0.01	-0.49
SHF of 15cm	0.24	0.49	-0.30	-0.09	0.25	0.53	-0.09	0.01	0.15	0.59	-0.23	-0.15	0.36	0.37	0.14	0.58
ALT	0.22	-0.40	0.40	0.27	0.32	-0.53	-0.05	0.02	0.29	0.49	0.70	0.25				
ΔI	0.49	-0.22	0.01	-0.08	0.50	-0.16	0.02	-0.16	0.29	0.31	0.24	-0.51	0.52	0.05	0.07	-0.03
SWC of 10 − 20cm													-0.31	0.45	0.22	0.47
SWC of 10 − 40cm	0.33	-0.20	0.50	0.25	-0.16	0.15	-0.16	0.73	0.28	-0.18	-0.41	0.53				
SWC of 50 − 160cm					0.23	-0.20	-0.16	0.55	0.31	-0.17	-0.32	0.41				
Precipitation					0.03	-0.04	0.63	0.35								
T_{soil} of 0 cm	0.43	-0.07	-0.20	-0.27	0.43	0.08	0.08	-0.07	0.37	0.07	0.19	-0.16	0.43	-0.35	-0.15	0.09
T_{soil} of 5 − 20 cm	0.44	-0.01	-0.17	-0.16									0.45	-0.28	0.00	0.28
T_{soil} of 5 − 40 cm					0.46	-0.05	0.04	-0.03	0.38	0.02	0.18	-0.17				
T_{soil} of 30 − 50cm	0.40	-0.23	-0.08	-0.04												
T_{soil} of 50 − 80cm					0.37	-0.36	0.00	0.01	0.37	-0.11	0.19	-0.14				
T_{soil} of 100 − 200cm					0.33	-0.34	0.01	-0.01	0.36	-0.14	0.08	0.00				
Percent of variance	0.63	0.23	0.08	0.04	0.70	0.18	0.07	0.02	0.69	0.17	0.08	0.04	0.75	0.21	0.02	0.01
Cumulative	0.63	0.86	0.94	0.98	0.70	0.88	0.95	0.97	0.69	0.86	0.94	0.98	0.75	0.96	0.98	0.99

Note: PC means principal component. Before PCA, SWC was divided for three parts, 10 – 20 cm, 10 – 40 cm, and 50 – 160 cm according to collinearity test in four seasons. T_{soil} was divided for six parts of T_{soil} of 0 cm, T_{soil} of 5 – 20 cm, T_{soil} of 5 – 40 cm, T_{soil} of 30 – 50 cm, T_{soil} of 50 – 80 cm, and T_{soil} of 60 – 200 cm according to collinearity test in different seasons.

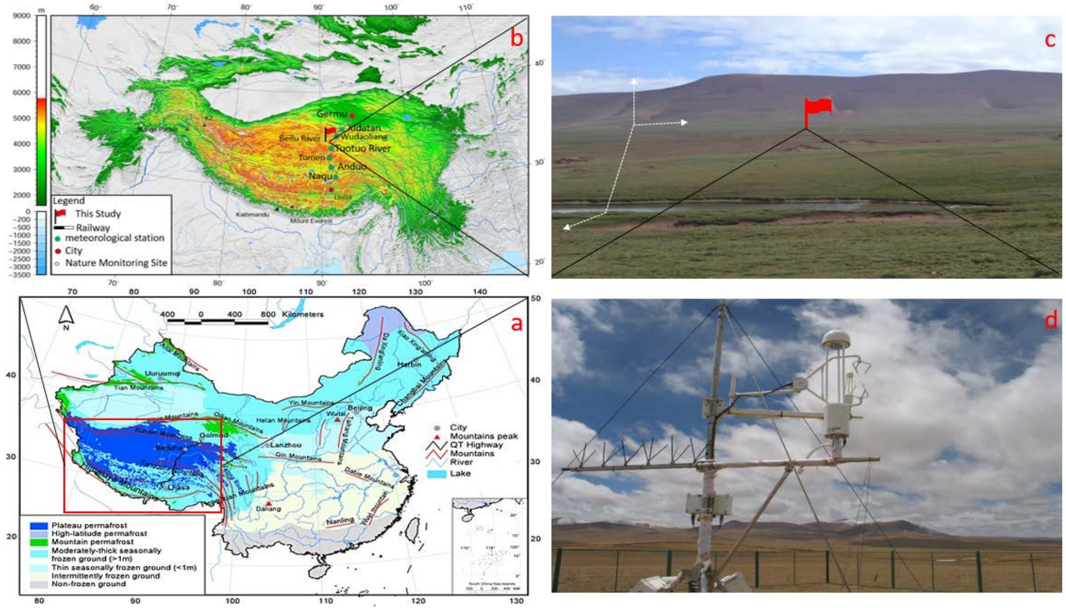

Figure 1. Geographic location of the study site: (a) is a map of China's permafrost distribution, and the red box marks the approximate location of the Qinghai–Tibet Plateau; (b) shows the study site location and meteorological stations along the Qinghai–Tibet railway; (c) is the photo showing the study site's topography and physiognomic. The small red flag in (c) is the eddy covariance tower location; (d) is the close–up shot of the LI–7700 for methane measurement. *Map boundary and location are approximate. Geographic features and the names do not imply any official endorsement or recognition*

Formatted: Width: 21.59 cm, Height: 27.94 cm

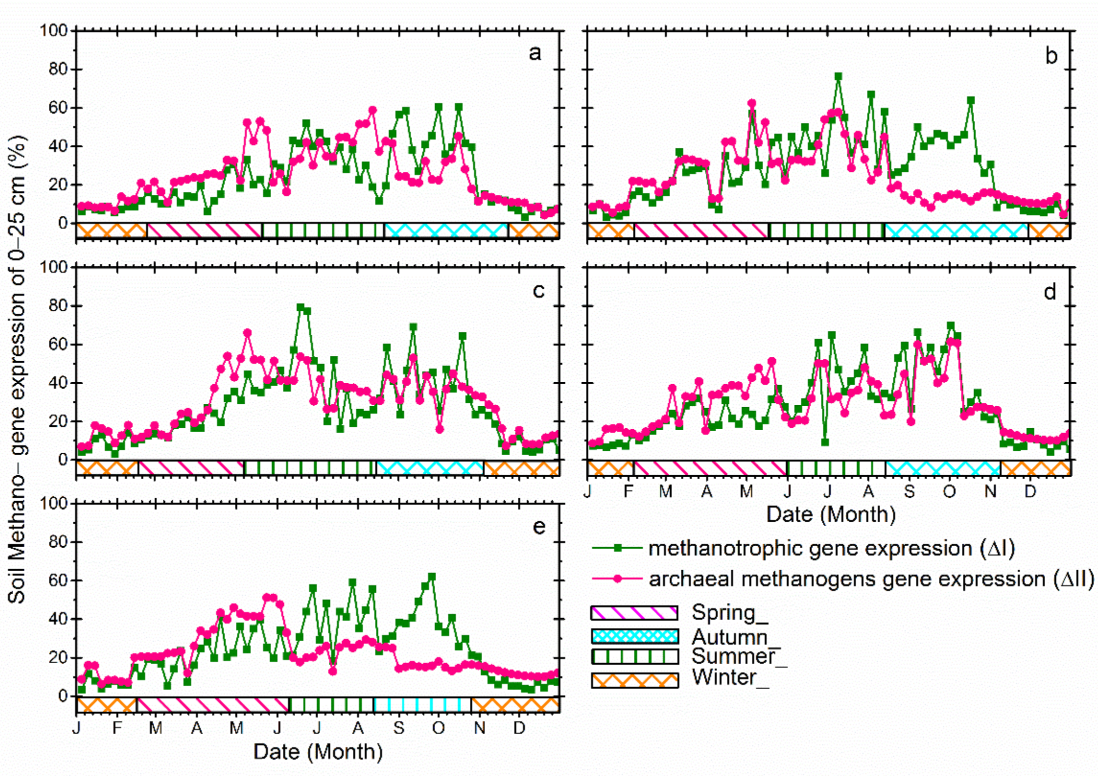

Soil Methano- gene expression of 0–25 cm (%)
a
b
c
d
e
Date (Month)
J F M A M J J A S O N D
methanotrophic gene expression (ΔI)
archaeal methanogens gene expression (ΔII)
Spring_
Autumn_
Summer_
Winter_

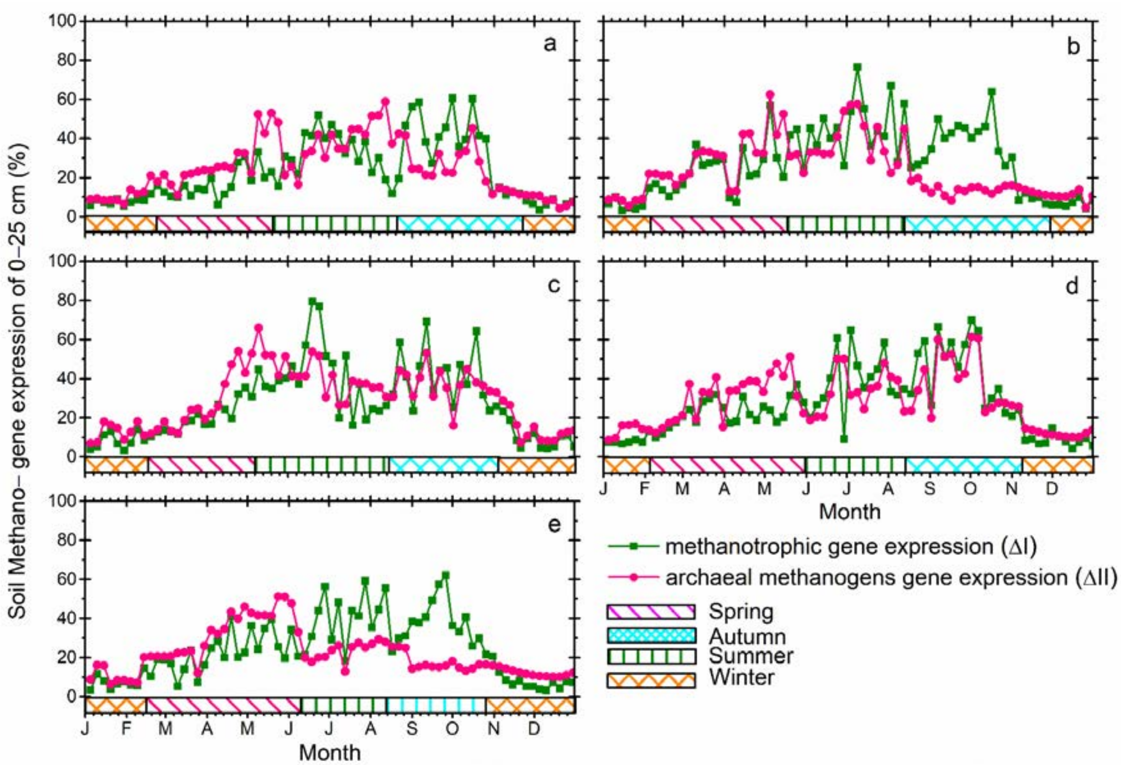

Figure 2. Annual patterns of soil methanogen−gene expression of 0 − 25 cm soil depth for years: (a) 2012, (b) 2013, (c) 2014, (d) 2015, and (e) 2016.

Comment [CA1]: Change “Spring_, Autumn_...” in the figure legend to “Spring, Autumn, ...”

Comment [CA2]: Also change the x-axis name to “Month” instead of “Date (Month)”.

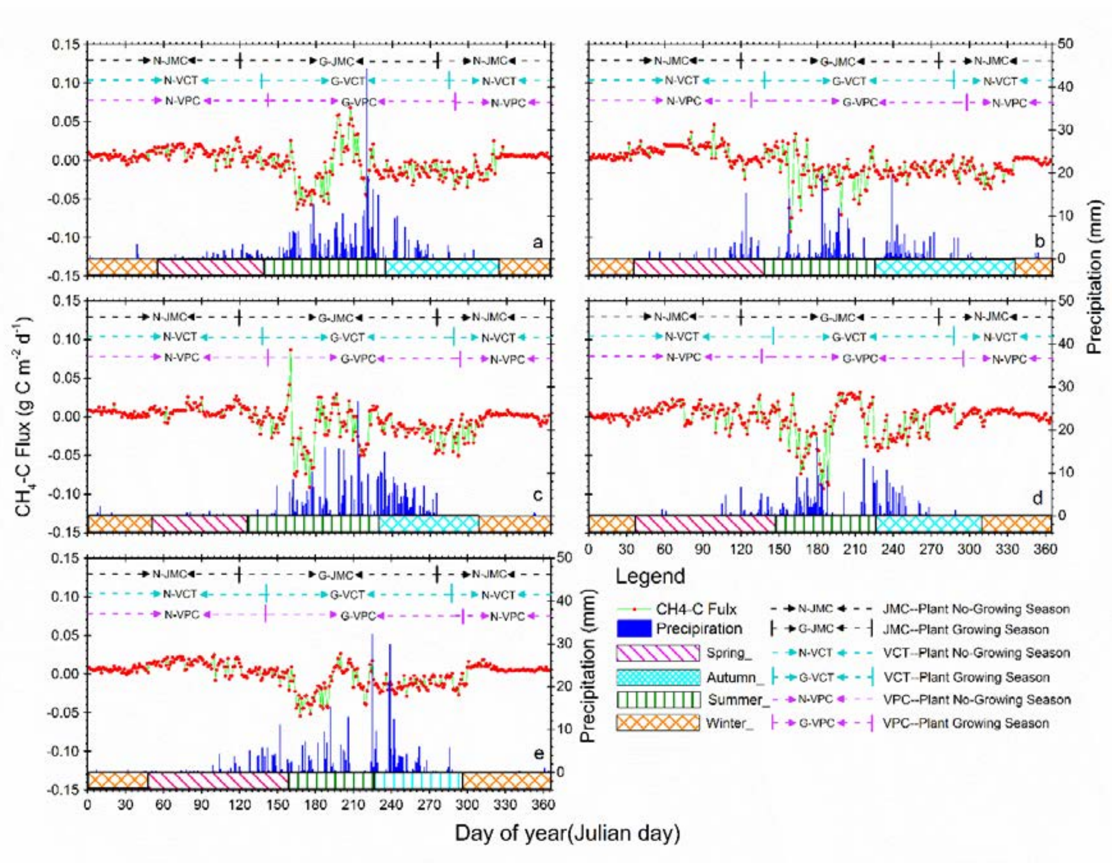

CH4-C Flux (g C m-2 d-1)
Precipitation (mm)
Day of year(Julian day)
N-JMC
G-JMC
N-VCT
G-VCT
N-VPC
G-VPC
a
b
c
d
e
Legend
CH4-C Fulx
Precipitation
Spring_
Autumn_
Summer_
Winter_
JMC--Plant No-Growing Season
JMC--Plant Growing Season
VCT--Plant No-Growing Season
VCT--Plant Growing Season
VPC--Plant No-Growing Season
VPC--Plant Growing Season

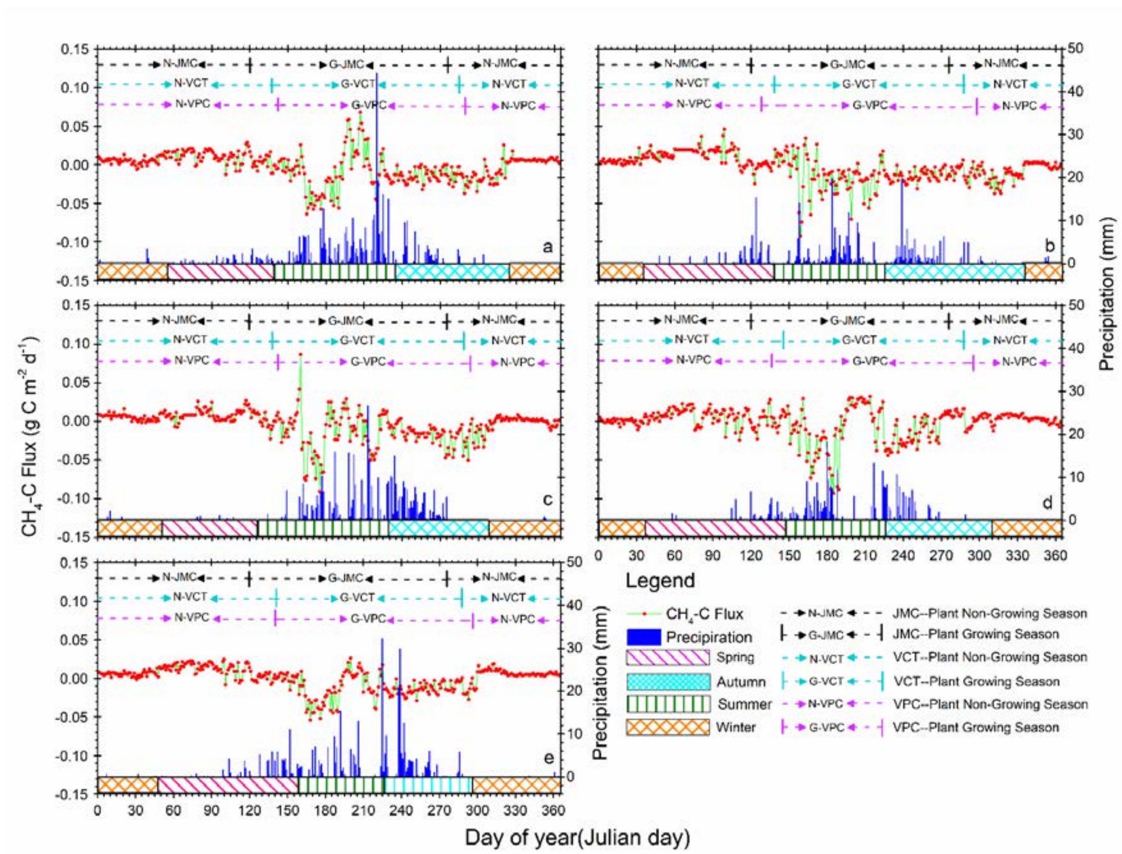

Figure 3. Annual patterns of ~~diel~~di~~urna~~el methane (CH_4) flux and precipitation variations from 2012 to 2016. Positive values indicate CH_4 release and negative values indicate CH_4 uptake by ecosystems. Red dots and light green lines are CH_4–C flux variation, and the deep blue histograms show ~~diel~~di~~urna~~el precipitation accumulation. Pink, olive, cyan, and orange blocks mean spring, summer, autumn, and winter seasons respectively, according to our new method of SMT (see Methods)~~,~~. Black, cyan, and pink dotted lines with bars separated the plant growing from non–growing seasons and stand for seasons by the method JMC, VCT, and VPC, respectively. Details about the methods JMC, VCT, and VPC can be found in ~~Text part~~section 3.2.

943

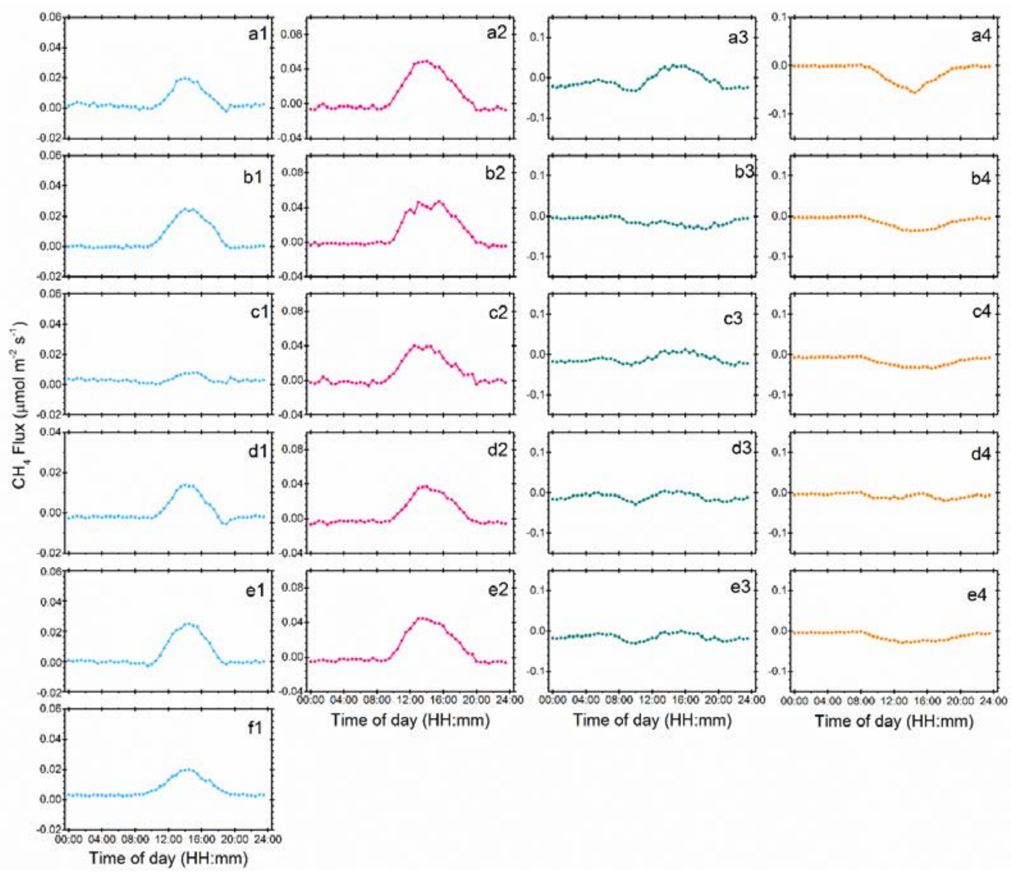

a1
a2
a3
a4
b1
b2
b3
b4
c1
c2
c3
c4
d1
d2
d3
d4
e1
e2
e3
e4
f1
CH4 Flux (µmol m-2 s-1)
Time of day (HH:mm)

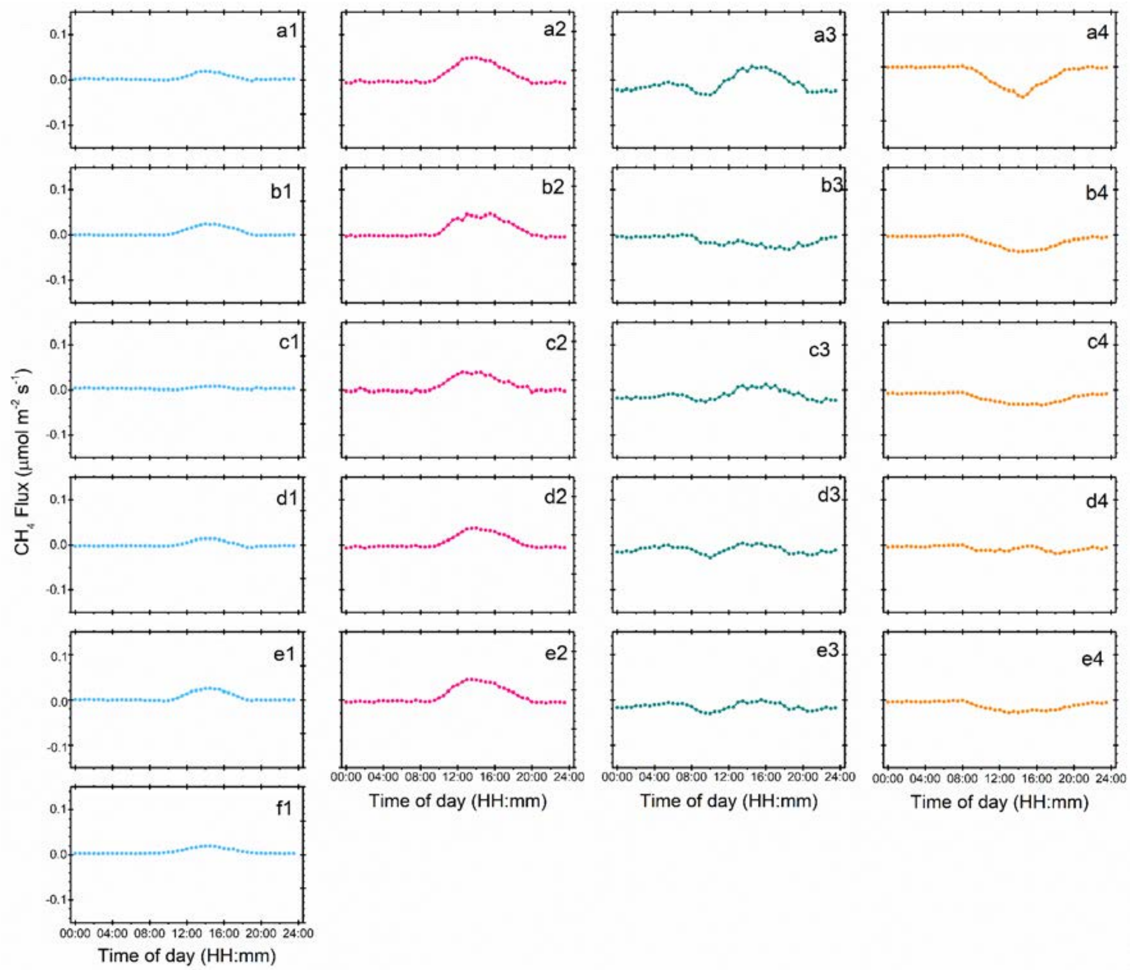

Figure 4. ~~Diel~~Di~~urna~~el CH_4 fluxes from 2012 to 2016 for different seasons. Blue, pink, green and orange, represent ~~winter~~winter, ~~spring~~spring, ~~summer~~summer, and ~~autumn~~autumn, respectively; (a1), (a2), (a3), and (a4) are for 2012; (b1), (b2), (b3), and (b4) are for 2013; (c1), (c2), (c3) and (c4) are for 2014; (d1), (d2), (d3), and (d4) are for 2015; (e1), (e2), (e3), (e4) and (f1) are for 2016.

Formatted: Line spacing: Multiple 1.08 li

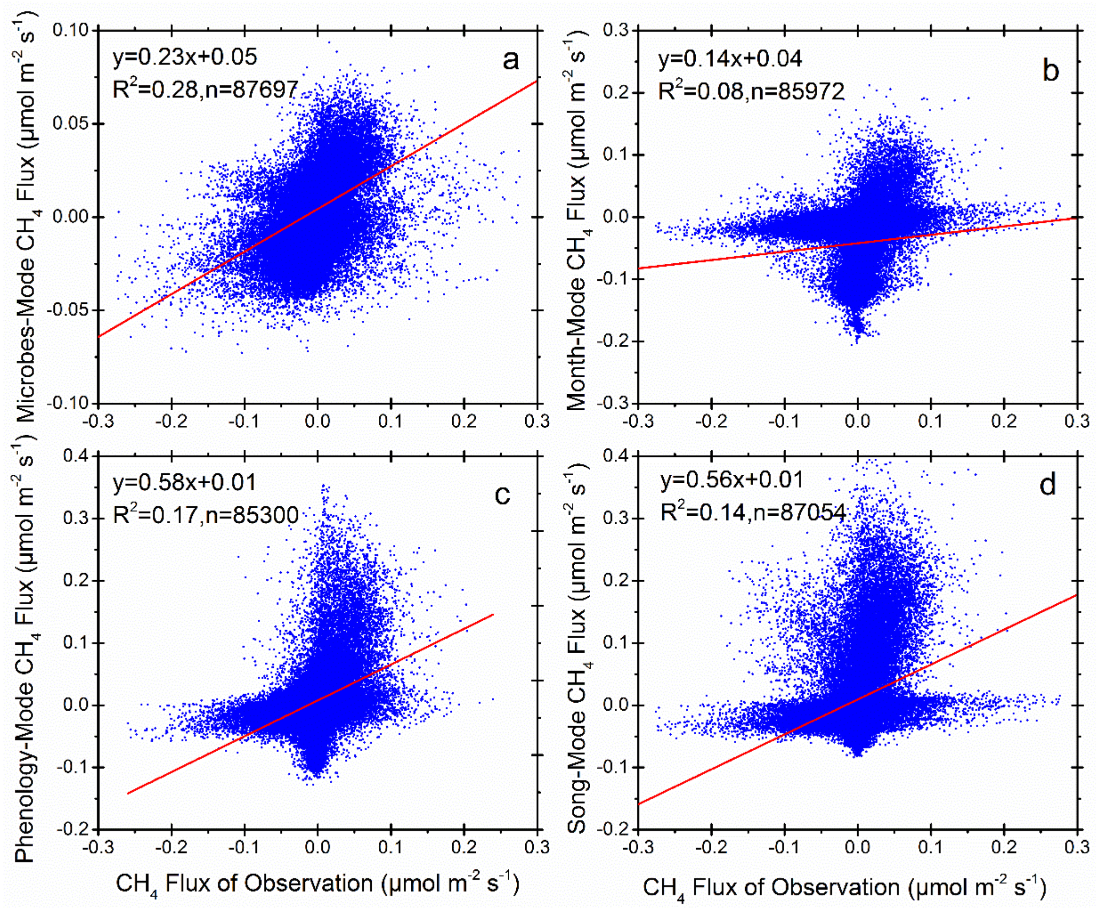

Figure 5. Regression comparison between observation and modeled methane fluxes with four different seasonal definitions and classification models. Panels (a), (b), (c), and (d) are for the SMT, JMC, VCT, and VPC methods, respectively.

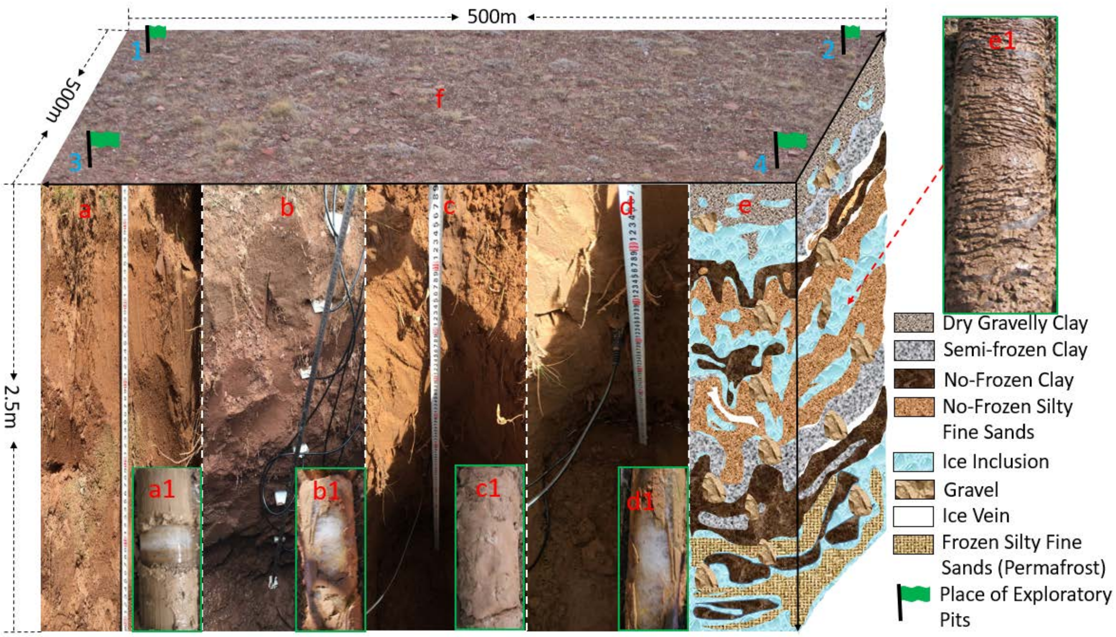

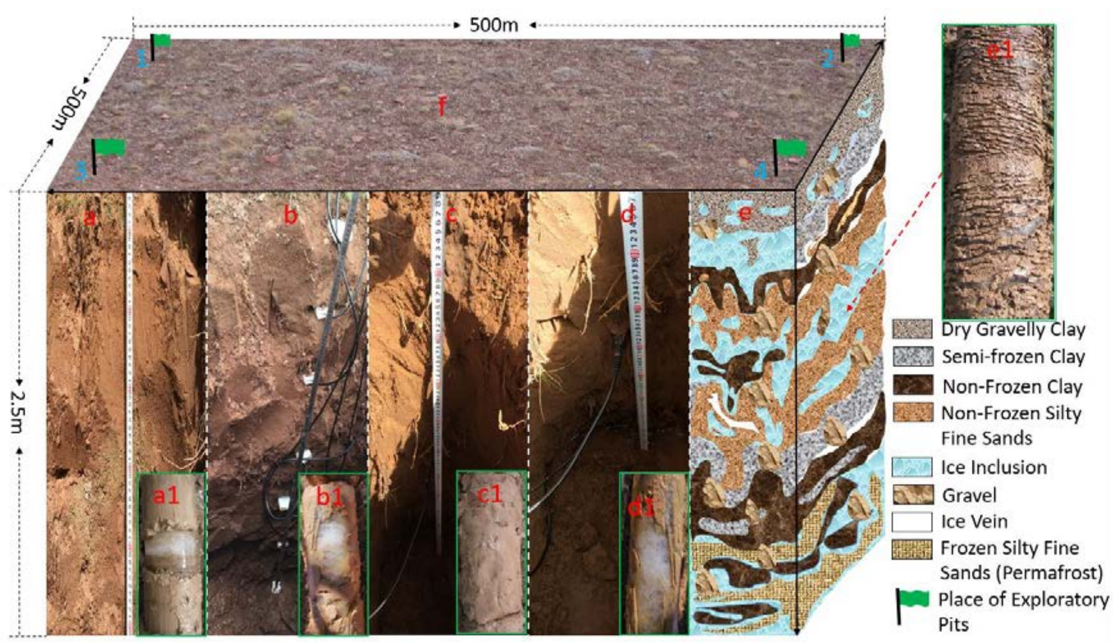

Figure 6. Location of exploratory pits and drillings in this study in autumn: (f) is photo of a typical ground surface (October 16th, 2014). Green flags represent the location for the soil survey by test pit~~sting~~ and drilling.

(a), (b), (c), and (d) ~~are test pitting sections for active layer~~show soil profiles of 0 − 250 cm depths ~~soil water content and temperature measured in~~ at the North (1), South (2), East (3), and West (4) corners of the eddy covariance footprint ~~North (1), South (2), East (3), and West (4) corners~~, respectively. (a1), (b1), (c1), and (d1) are drilling cores, with clear ice (white) in (a1), (b1), and (d1), but not in (c1); (e) provides an illustration that combines results from drillings, test ~~pitting~~ pits and multi–channel ground–penetrating radar (Malå Geoscience, Sweden) for active layer variations in permafrost area during the autumn season; and (e1) is a core sample of the same drilling (October 16th, 2014).

Formatted: Highlight

Formatted: Highlight

Formatted: Highlight

Formatted: Highlight

Formatted: Highlight

Supplement

Supplementary Table 1 Seasonal soil water content (SWC, %) of ~~winter~~ winter, ~~spring~~ spring, ~~summer~~ summer, and ~~autumn~~ autumn from 2012 to 2016.

Seasonal	Period	10 cm	20 cm	40 cm	80cm	160cm
		Soil Water Content (SWC), %				
~~Winter~~ Winter	2012 early	0.11	0.08	0.07	0.11	0.14
	2012-2013	0.10	0.08	0.07	0.11	0.16
	2013-2014	0.10	0.08	0.07	0.11	0.13
	2014-2015	0.10	0.08	0.07	0.11	0.17
	2015-2016	0.10	0.08	0.07	0.11	0.16
	2016 later	0.10	0.08	0.07	0.12	0.19
	Average	0.10	0.08	0.07	0.11	0.16
~~Spring~~ Spring	2012	0.13	0.09	0.08	0.11	0.13
	2013	0.12	0.09	0.08	0.11	0.13
	2014	0.12	0.08	0.07	0.11	0.13
	2015	0.13	0.09	0.08	0.11	0.14
	2016	0.12	0.09	0.08	0.13	0.15
	Average	0.12	0.08	0.08	0.11	0.14
~~Summer~~ Summer	2012	0.18	0.11	0.10	0.17	0.27

	2013	0.16	0.11	0.11	0.19	0.25
	2014	0.16	0.10	0.10	0.16	0.24
	2015	0.16	0.10	0.10	0.19	0.28
	2016	0.16	0.10	0.09	0.18	0.28
	Average	0.17	0.10	0.10	0.18	0.26
~~Autumn~~ Autumn	2012	0.14	0.09	0.08	0.14	0.21
	2013	0.14	0.09	0.09	0.15	0.20
	2014	0.16	0.10	0.10	0.16	0.22
	2015	0.15	0.10	0.09	0.15	0.21
	2016	0.16	0.10	0.09	0.16	0.21
	Average	0.15	0.10	0.09	0.15	0.21

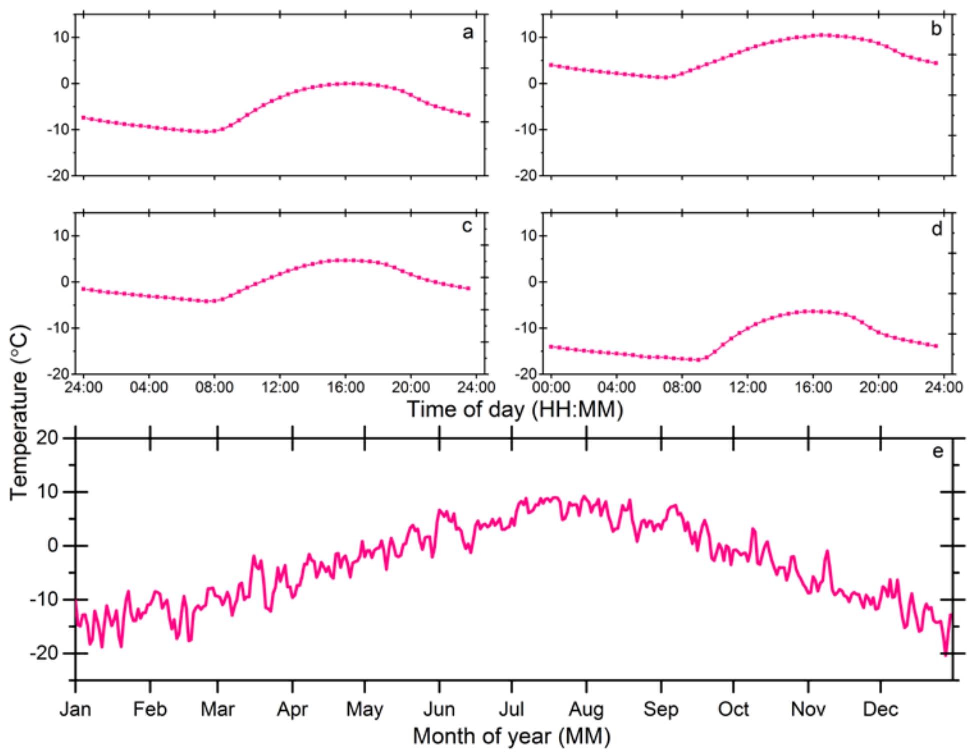

Supplementary Figure 1. Air temperature (T_{air}) measured ~~of~~ 3 meters above the ground surface: (a), (b), (c), and (d) are half–hourly ~~scale~~ mean values in ~~spring~~spring, ~~summer~~summer, ~~autumn~~autumn, and ~~winter~~winter, respectively; (e) shows ~~diel~~diurnael–scale mean values from 2012 to 2016.

Formatted: Subscript

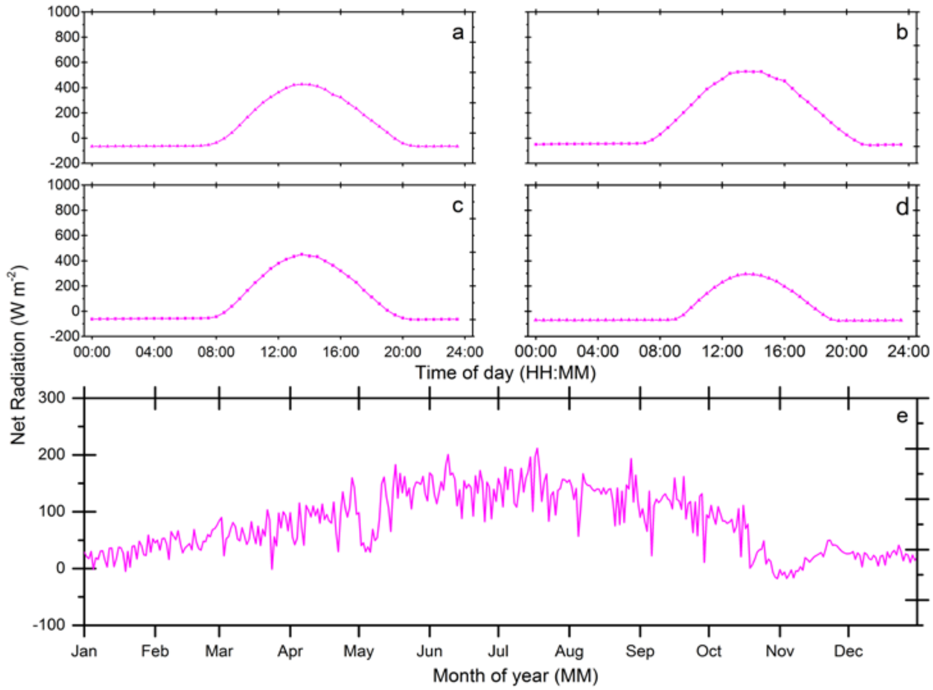

Supplementary Figure 2. Net radiation (Rn) of measured 3 meters above the ground surface: (a), (b), (c), and (d) are half–hourly scale mean values in springspring, summersummer, autumnautumn, and winterwinter, respectively; (e) shows dieldiurnael–scale mean values from 2012 to 2016.

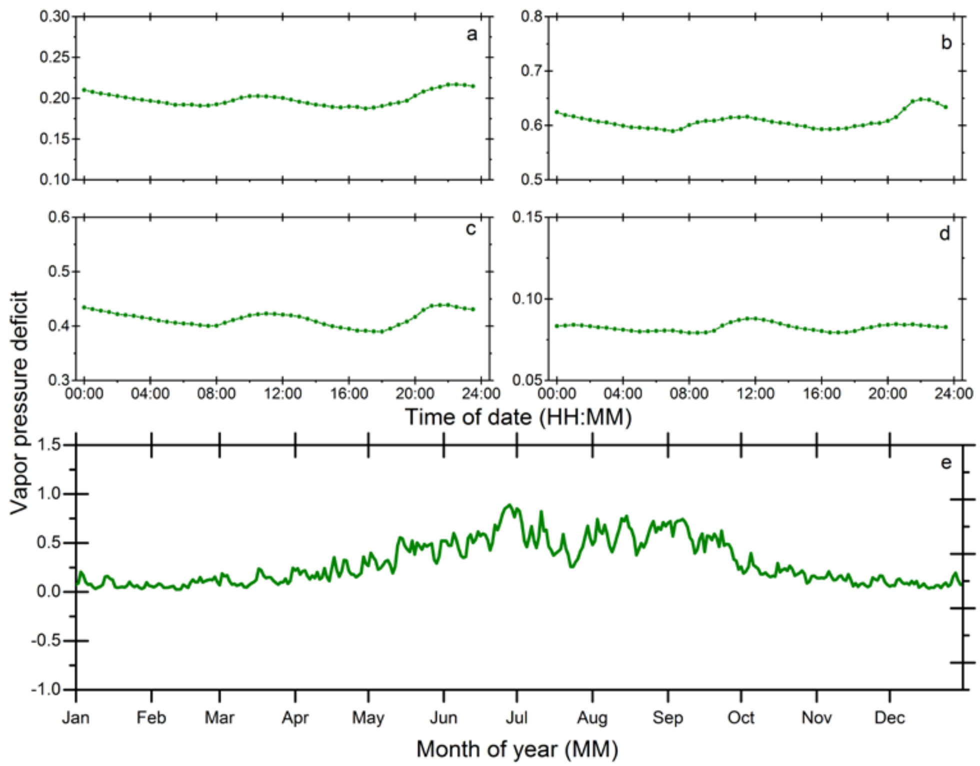

Supplementary Figure 3. Vapor pressure deficit (VPD) ~~of~~ measured 3 meters above the ground surface: (a), (b), (c), and (d) are half–hourly ~~scale~~ mean values in ~~spring~~spring, ~~summer~~summer, ~~autumn~~autumn, and ~~winter~~winter, respectively; (e) shows ~~diel~~di~~urna~~el ~~- scale~~ mean values from 2012 to 2016.

993

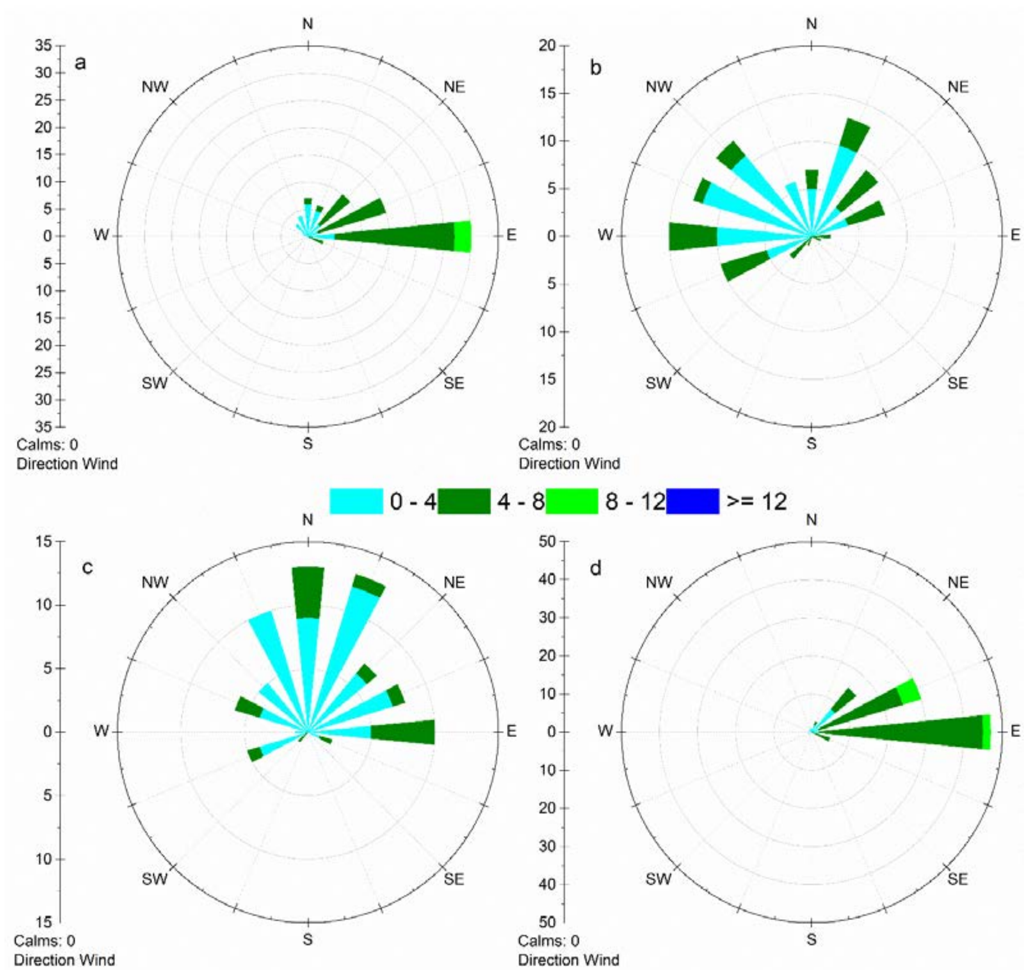

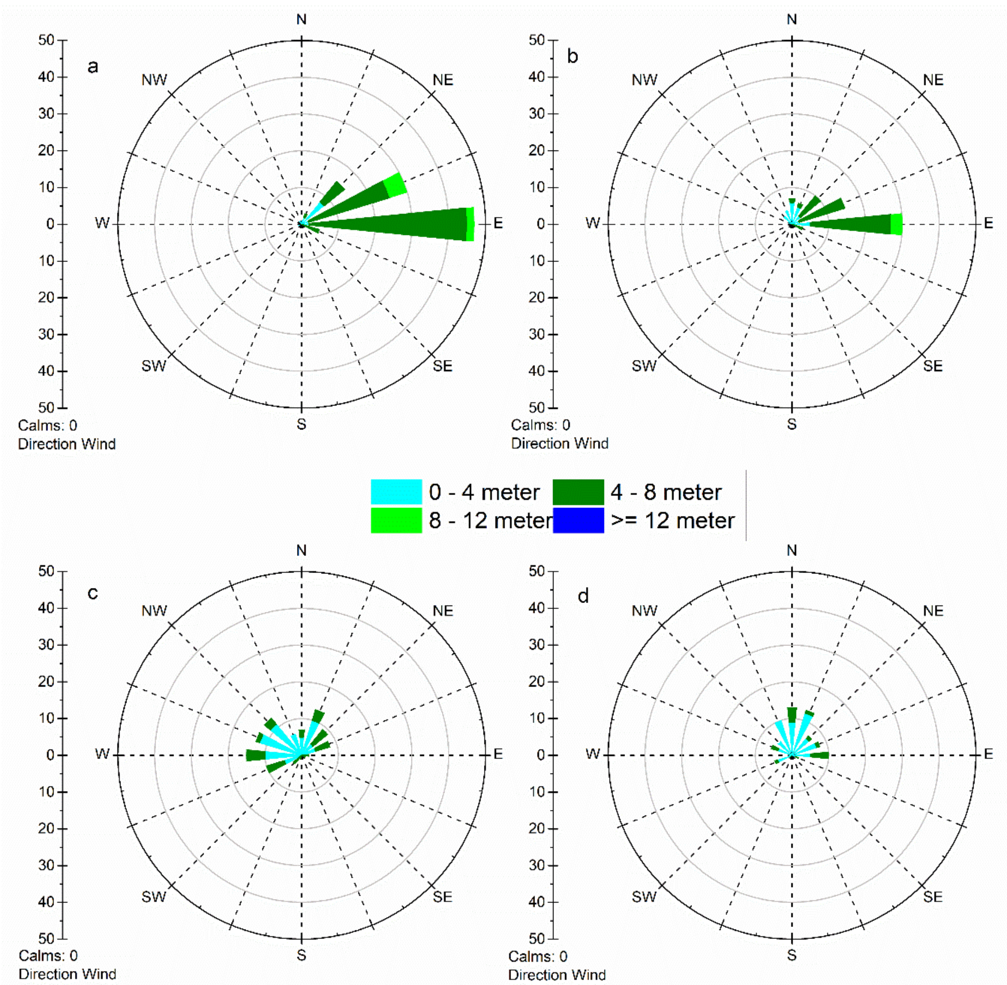

Supplementary Figure 4. ~~Diel~~Di~~urnae~~l mean of wind speed and direction between 2012 and 2016: (a) is winter, (b) is spring, (c) is summer, and (d) is autumn. ~~-~~Note the direction of wind means the direction wind blows *from*. All data are presented as mean values with standard deviations (mean ± standard deviation).

Formatted: Font: Italic

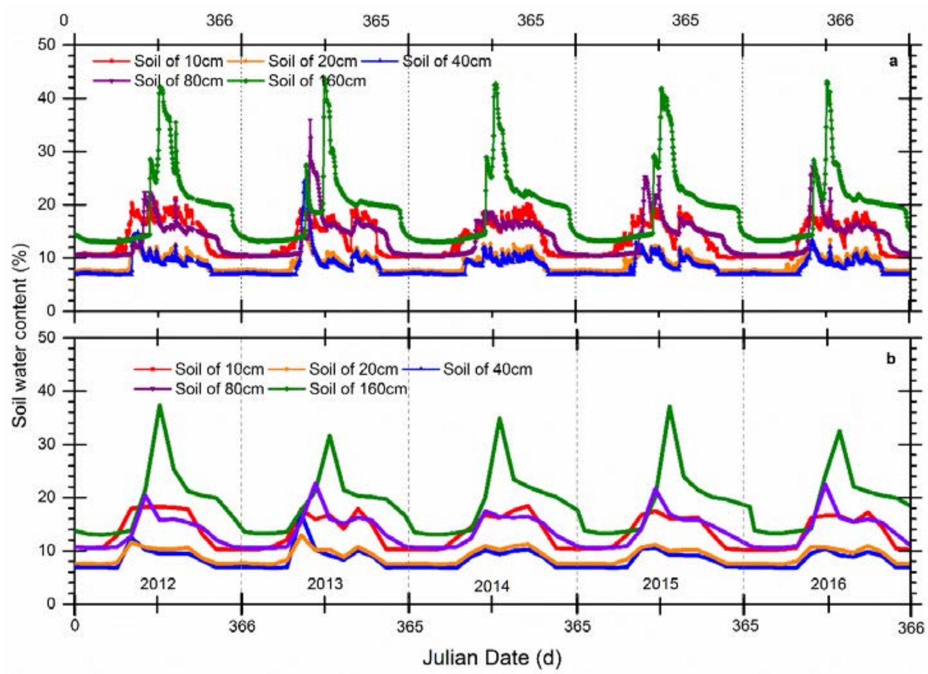

Supplementary Figure 5. Comparison between soil water content (SWC) of two different time resolutions from 2012 to 2016, (a) is the half–hourly ~~scale~~ SWC at soil depths of 10 cm, 20 cm, 40 cm, 80 cm, and 160 cm; and (b) is the 4–hourly mean SWC for the same depths.

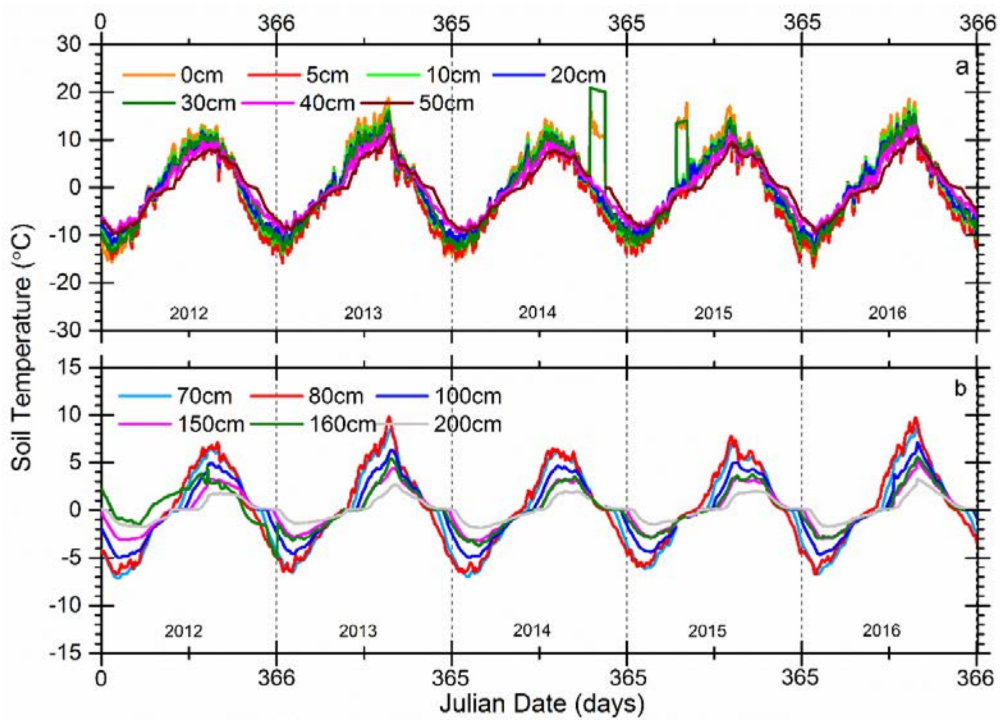

Supplementary Figure 6. Half–hour measurements ~~scale~~ of 0 − 200 cm soil temperature (T_{soil}) variations from 2012 to 2016, (a) is for soil depths of 0 cm, 5 cm, 10 cm, 20 cm, 30 cm, 40 cm, 50 cm, (b) is for soil depth of 70 cm, 80 cm, 100 cm, 150 cm, 160 cm, and 200 cm.

Formatted: Subscript

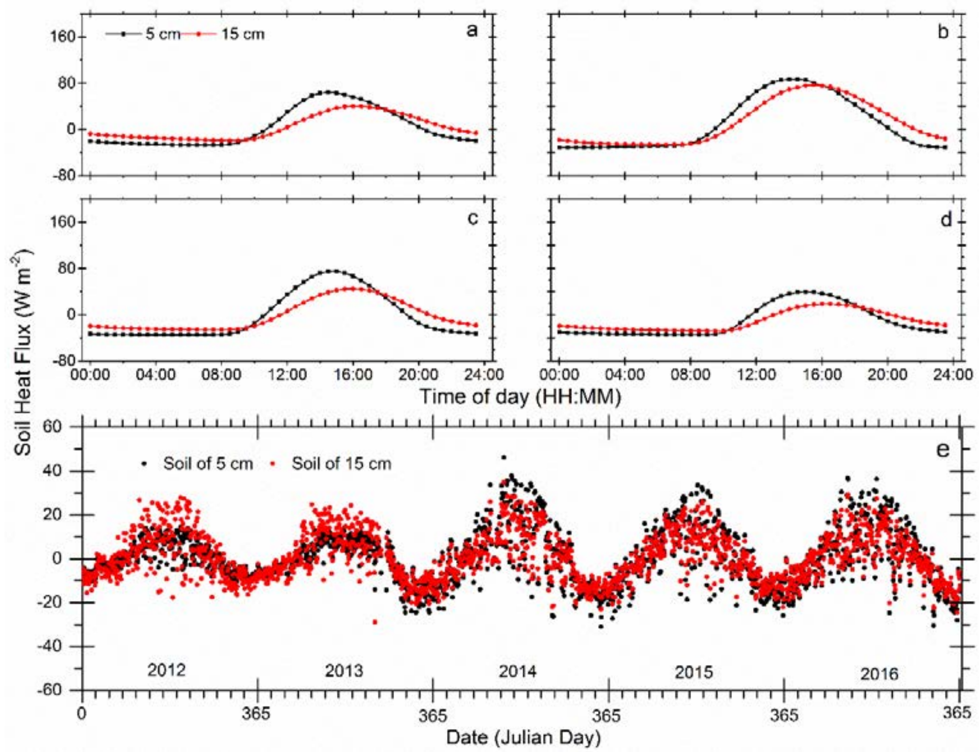

Supplementary Figure 7. Soil heat flux (SHF) at depth of 5 cm and 15 cm: (a), (b), (c), and (d) are half–hourly ~~scale~~ mean values in ~~spring~~spring, ~~summer~~summer, ~~autumn~~autumn, and ~~winter~~winter, respectively; (e) shows ~~diel~~di~~urna~~el ~~–scale~~ mean values from 2012 to 2016.

.

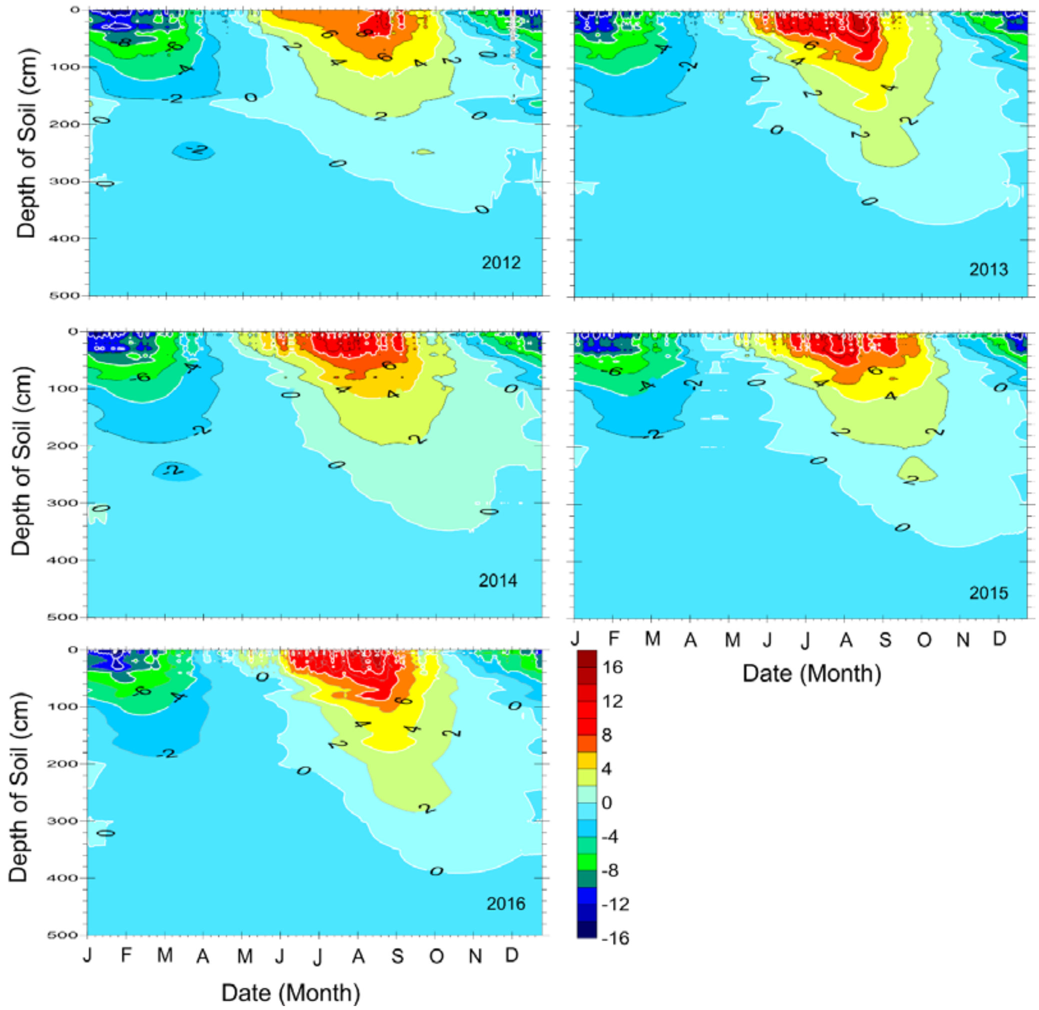

Supplementary Figure 8. Characteristics of the seasonal freezing and thawing processes of the active layer for years: 2012, 2013, 2014, 2015, and 2016. Different colors represent the soil temperature gradients from -16 °C to 20 °C. The depth of 0 °C represent the active layer thickness (ALT).

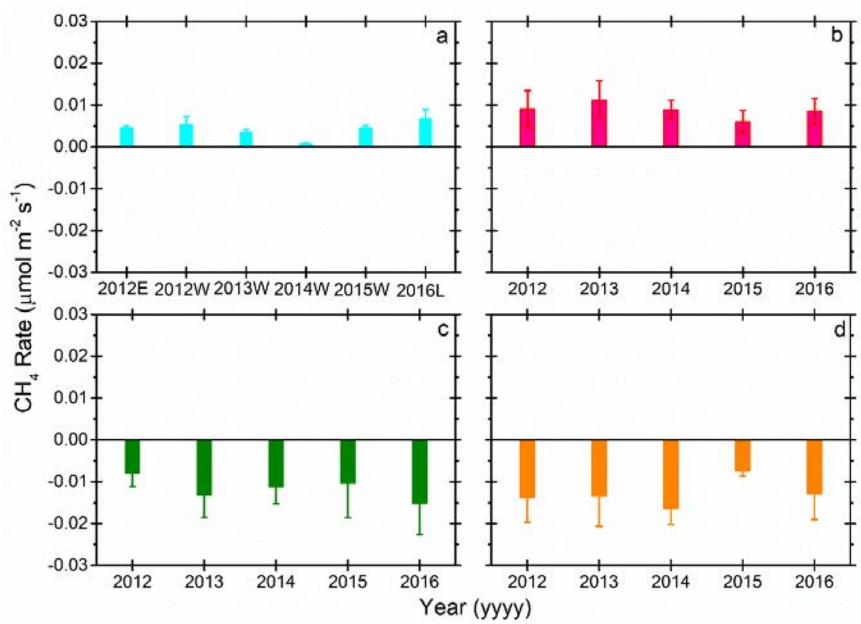

Supplementary Figure 9. Seasonal CH_4 rate mean value from 2012 to 2016: (a) is ~~winter~~winter, (b) is ~~spring~~spring, (c) is ~~summer~~summer, and (d) is ~~autumn~~autumn. In the (a), 2012E is started from January 1st, 2012 and ended on February 17th, 2012; 2012W is started from 19th November, 2012 to 4th February, 2013; 2013W is started from 1st December, 2013 to 17th February, 2014; 2014W is started from 6th November, 2014 to 4th February, 2015; 2015W is started from 9th November, 2015 to 15th February, 2016; 2016L is started from October 26th, 2016 and ended on December 31st, 2016. All data are presented as mean values with standard deviations (mean ± standard deviation).

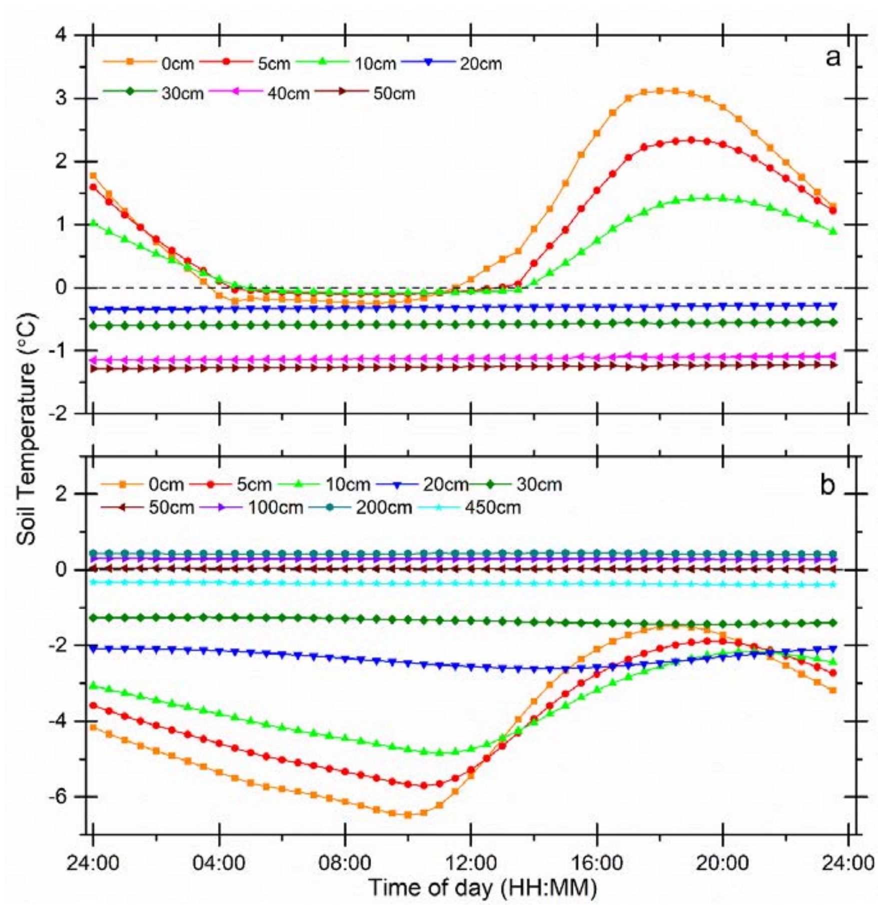

Supplementary Figure 10. ~~Average~~ Mean half–hourly values ~~scale~~ of 0 − 450 cm soil temperature (T_{soil}) ~~diel variations~~ from 2012 to 2016, (a) is for ~~spring~~ spring, (b) is for ~~autumn~~ autumn. Note~~dly~~, that during spring~~, the~~ T_{soil} of 100cm, 200cm, 450cm is always ~~were all~~ below -2 ℃ and during ~~autumn~~ autumn the T_{soil} of 40cm almost overlap to T_{soil} ~~of~~ with 50cm~~,~~ . ~~to~~ To make the figure more readable, ~~clearly,~~ we removed the T_{soil} values of 100cm, 200cm, 450cm in figure (a) and removed the T_{soil} values of 40cm for figure (b).

Formatted: Subscript

Formatted: Subscript

Formatted: Subscript

Formatted: Subscript

Formatted: Subscript

Formatted: Subscript

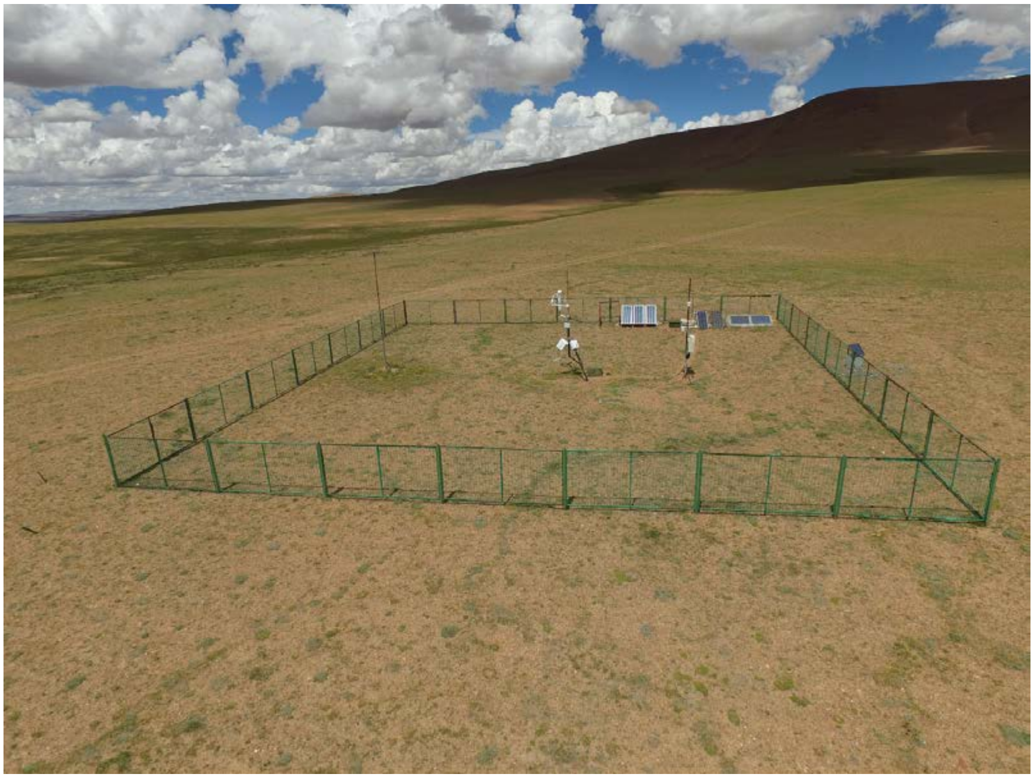

Supplementary Figure 11. A bird's eye view of the eddy covariance site ~~in~~ at the Beilu'he station